

An FFT-based algorithm for efficient computation of Green's functions for the Helmholtz and Maxwell's equations in periodic domains

Bo Zhang* Ruming Zhang†

Abstract

The integral equation method is widely used in numerical simulations of 2D/3D acoustic and electromagnetic scattering problems, that needs a large number of values of the Green's functions. A significant topic is the scattering problems in periodic domains, that the corresponding Green's functions are quasi-periodic. The quasi-periodic Green's functions are defined by series that converge too slowly to be used for calculations. Many mathematicians have developed several efficient numerical methods to calculate quasi-periodic Green's functions. In this paper, we will introduce a new FFT-based fast algorithm to compute the 2D/3D quasi-periodic Green's functions for both Helmholtz equations and Maxwell's equations. The convergence results and error estimates are also investigated in this paper. At the end of this paper, the numerical examples will be given to show that when large number of values are needed, the new algorithm is very competitive.

Keywords: FFT-based algorithm, periodic domain, Green's function, interpolation, convergence

1 Introduction

In the scattering theory, the integral equation method is an efficient and widely used method for numerical simulations. During the numerical procedure to solve the integral equations, a large number of values of the Green's functions and their derivatives are needed. In recent years, many mathematicians are interested in the topic that the acoustic/electromagnetic fields scattered in periodic domains with quasi-periodic incident waves, where the corresponding Green's functions are quasi-periodic. In this case, the quasi-periodic Green's functions, that are defined by slowly convergent series, are always very difficult to evaluate. In this paper, we will develop a new FFT-based method to approximate the Green's functions in 2D periodic domains or 3D doubly periodic domains, for Helmholtz equations and Maxwell's equations numerically.

1) The quasi-periodic Green's function $G(x)$ for Helmholtz equations in 2D domains.

*LSEC and Institute of Applied Mathematics, AMSS, Chinese Academy of Sciences, Beijing, 100190, China and School of Mathematical Sciences, University of Chinese Academy of Sciences, Beijing 100049, China (b.zhang@amt.ac.cn)

†Center for Industrial Mathematics, University of Bremen, Bremen 28359, Germany (rzhang@uni-bremen.de); corresponding author

Assume that the 2D domain is 2π -periodic in x_1 -direction, and the incident wave u^i is α -quasi-periodic, i.e. $u^i(x_1 + 2\pi, x_2) = e^{i2\pi\alpha}u^i(x_1, x_2)$. The corresponding Green's function is also α -quasi-periodic and can be defined by the basic image expansion

$$G(x) = \frac{i}{4}H_0^{(1)}(k|x|) + \frac{i}{4} \sum_{n \neq 0, n \in \mathbb{Z}} e^{i2\pi\alpha n} H_0^{(1)}(kr_n), \quad (1.1)$$

where $r_n = \sqrt{(x_1 - 2\pi n)^2 + x_2^2}$. It can also be defined by the basic eigenfunction expansion [14]:

$$G(x) = \frac{i}{4\pi} \sum_{n=-\infty}^{\infty} \frac{1}{\beta_n} \exp(i\alpha_n x_1 + i\beta_n |x_2|), \quad (1.2)$$

where $\alpha_n = \alpha + n$,

$$\beta_n = \begin{cases} \sqrt{k^2 - \alpha_n^2}, & \text{if } |\alpha_n| \leq k, \\ i\sqrt{\alpha_n^2 - k^2}, & \text{otherwise.} \end{cases}$$

2) The doubly quasi-periodic Green's function $G_d(x)$ for Helmholtz equations in 3D domains.

Assume that the 3D domain is 2π -periodic in both x_1 - and x_2 -directions, and the incident wave u^i is doubly quasi-periodic, i.e., for any integers m_1, m_2 , $u^i(x_1 + 2m_1\pi, x_2 + 2m_2\pi, x_3) = e^{i2m_1\pi\alpha_1}e^{i2m_2\pi\alpha_2}u^i(x_1, x_2, x_3)$. Then the corresponding Green's function is also doubly quasi-periodic and can be defined by the basic eigenfunction expansion [16]:

$$G_d(x) = \frac{i}{8\pi^2} \sum_{n_1, n_2 \in \mathbb{Z}} \frac{1}{\beta_{n_1, n_2}} \exp(i\alpha_{1, n_1} x_1 + i\alpha_{2, n_2} x_2 + i\beta_{n_1, n_2} |x_3|), \quad (1.3)$$

where $\alpha_1, \alpha_2 \in \mathbb{R}$, $\alpha_{1, n_1} = \alpha_1 + n_1$, $\alpha_{2, n_2} = \alpha_2 + n_2$

$$\beta_{n_1, n_2} = \begin{cases} \sqrt{k^2 - \alpha_{1, n_1}^2 - \alpha_{2, n_2}^2}, & \text{if } \alpha_{1, n_1}^2 + \alpha_{2, n_2}^2 \leq k^2, \\ i\sqrt{\alpha_{1, n_1}^2 + \alpha_{2, n_2}^2 - k^2}, & \text{otherwise.} \end{cases}$$

3) The doubly quasi-periodic Green's tensor $\mathbb{G}(x)$ for Maxwell's equations in 3D domains.

The doubly quasi-periodic Green's tensor $\mathbb{G}(x)$ for Maxwell equations is a 3×3 matrix defined by $G_d(x)$:

$$\mathbb{G}(x) = G_d(x)\mathbb{I} + \frac{1}{k^2} \nabla \nabla \cdot (G_d(x)\mathbb{I}) \quad (1.4)$$

where \mathbb{I} is the 3×3 identity matrix. $\mathbb{G}(x)$ is composed by $G_d(x)$ and its second order derivatives. So the numerical method of \mathbb{G} comes directly from that of $G_d(x)$.

In this paper, we will discuss the numerical method to calculate the functions $G(x)$, $G_d(x)$ and $\mathbb{G}(x)$ in 2D/3D domains. In this paper, we always assume that the cases we consider are away from Wood anomalies, i.e., $\beta_n \neq 0$ for 2D case and $\beta_{n_1, n_2} \neq 0$ for 3D case. The definition (1.1) is the sum of Hankel functions that converges very slowly, which will cost a lot of time in calculation. From the definition of $G(x)$ in (1.2), the function is defined by the series of exponential functions, and converges rapidly when x is away from the line $x_2 = 0$. When $x_2 \rightarrow 0$, the series converges slowly, and this method fails. Similarly, the direct calculation from the definition (1.3) of $G_d(x)$ fails when $x_3 \rightarrow 0$.

Many methods have been developed to evaluate the Green's function in 2D and 3D domains, such as the Kummer's transformation, the Ewald method, the Lattice sums and the integral representations. C. M. Linton compared several methods in [14] in 2D doamins and [16] in 3D domains. In the two papers, he gave the conclusions that if only a few values are needed, the Ewald's method is the most efficient method, while if a large number of values are needed, the lattice sums is better. There are many papers concerns with the Lattice sums method and the Ewald's method both, see [9, 30, 23, 5, 20, 28, 1, 11, 21, 26] for 2D cases, and see [18, 6, 11, 21, 26, 20, 28, 20, 15, 25, 17] for 3D cases. There are also some other methods considering the numerical evaluation of the Green's functions, see [2, 22, 3, 4] for example. Especially, the cases that near or at the Wood anomalies, which are very difficult to be approximated, have been considered in [22, 3, 4]. For very large k 's ($> 10^5$), H. Kurkcu and F. Reitich gave the NA method in 2D domains, which comes from the integral representations, see [10]. However, all of the known methods have their advantages and limitations. Take the Lattice sums, the Ewald method and the NA method in 2D domain for example. The Lattice sums converges very fast, especially when the wave number k is small enough. This makes it the best method to calculate large number of values in this case. But the convergence radius of the lattice sums depends on the wave number k . If k becomes larger, the lattice sums needs more terms for the accuracy, which involves more evaluations of Hankel functions and Bessel functions, thus needs more time. What is worse, when k is gets larger ($k \geq 50$), the lattice sums only converges in a very small disk, so the method no longer works for most points. However, the Ewald's method is always able to achieve expected accuracy for both small and large k 's, but it costs much more time. So it might not be a good choice when a large number of values are needed. The NA method for 2D domains is of higher efficiency than the other methods, when k is very large ($> 10^5$). However, when k is not so large, i.e. $k \sim 100$, its efficiency is even worse than the Ewald method, thus not suitable for the calculation. What we aim to seek is a method that converges for any k and spend less time than known methods. In this paper, we develop a new FFT-based method that converges for any k and is very efficient when large number of values are needed.

Our method is based on FFT. First, we will transform the Green's function $G(x)$ ($G_d(x)$) into a periodic function in 2D (3D) domains. Then we can compute its Fourier series analytically by direct calculations. The idea is from [27], in which Fourier series of the Hankel function are used to solve Lippmann-Schwinger equations in 2D domains. The method was extended to 2D periodic domains in [24] and to 3D domains in [8, 12]. Note that the Green's functions are singular at zero, the Fourier series converge very slowly. For a better convergence, we will remove the singularity to get the smooth enough modified functions. The Fourier coefficients of the modified functions are computed numerically and applied to obtain the values on the grid points from IFFT. Then the values of the modified functions on random points can be evaluated simply by interpolation. It is now easy to obtain the values of the Green's functions. The derivatives of the Green's functions could be calculated in the similar way.

This paper is organized as follows. In Section 2, we will give a new FFT-based algorithm to calculate the Green's function $G(x)$ in two dimensions. In section 3, the FFT-based algorithm is applied to calculate the Green's function $G_d(x)$ for Helmholtz equation in three dimensions. In Section 4, The numerical method to calculate the Green's tensor $\mathbb{G}(x)$ will be studied. In Section 5, we will give the convergence results and error estimates for the numerical methods. In section 6, we will show some numerical examples of the calculation of $G(x)$, $G_d(x)$, $\mathbb{G}(x)$.

2 The FFT-based algorithm in two dimensions

2.1 Periodization and Fourier coefficients

Set $D_c = [-\pi, \pi] \times [-c, c]$, where c is a positive real number which is chosen so that for $|x_2| \geq c$ the series expansion (1.2) can be directly used to compute $G(x)$ efficiently. Thus, we will develop an efficient method to compute the Green's function $G(x)$ for $x \in D_c$.

From the series expansion (1.2) it follows that

$$e^{-i\alpha x_1} G(x) = \frac{i}{4\pi} \sum_{n=-\infty}^{\infty} \frac{1}{\beta_n} \exp(inx_1 + i\beta_n|x_2|)$$

which is 2π -periodic in the x_1 -direction.

Let $\tilde{c} > c$ and let $\mathcal{X}(t)$ be a smooth cut-off function for $t \geq 0$ such that $\mathcal{X}(t) = 1$ for $0 \leq t \leq c$ and $\mathcal{X}(t) = 0$ for $t \geq (c + \tilde{c})/2$. Define a new function $K(x)$:

$$K(x) = e^{-i\alpha x_1} G(x) \mathcal{X}(|x_2|) \quad \text{for } x \in \mathbb{R} \times [-\tilde{c}, \tilde{c}]$$

Then $K(x)$ is zero for $x \in [-\pi, \pi] \times [(c + \tilde{c})/2, \tilde{c}]$ and $x \in [-\pi, \pi] \times [-\tilde{c}, -(c + \tilde{c})/2]$. We extend K into a $2\tilde{c}$ -periodic function in x_2 -direction which is denoted by K again. Then K is now a bi-periodic function in \mathbb{R}^2 . Note that K is smooth in $D_{\tilde{c}} \setminus \{0\}$ and

$$G(x) = e^{i\alpha x_1} K(x) \quad \text{for } x \in D_c. \quad (2.1)$$

We now calculate the Fourier coefficients of K . To do this, we divide the rectangular domain $D_{\tilde{c}}$ uniformly into $2N \times 2N$ small rectangles. Set $S_N = \{j = (j_1, j_2) \in \mathbb{Z}^2 : -N \leq j_1, j_2 < N\}$. The grid points are denoted by $x_j = (x_{1j_1}, x_{2j_2})$, where $x_{1j_1} = (\pi/N)j_1$, $x_{2j_2} = (\tilde{c}/N)j_2$ with $j = (j_1, j_2) \in S_N$. Define the Fourier basis of $L^2(D_{\tilde{c}})$ by

$$\phi_j(x) = \frac{1}{2\sqrt{\pi\tilde{c}}} \exp(ij_1 x_1 + ij_2 \pi x_2 / \tilde{c}), \quad j = (j_1, j_2) \in \mathbb{Z}^2$$

Then $K(x)$ can be approximated by $K_N(x)$:

$$K_N(x) = \sum_{j \in S_N} \hat{K}_j \phi_j(x)$$

where \hat{K}_j is the j -th Fourier coefficient of K . By a direct calculation \hat{K}_j is given by

$$\begin{aligned} \hat{K}_j &= \int_{D_{\tilde{c}}} K(x) \bar{\phi}_j(x) dx = \int_{D_{\tilde{c}}} K(x) \phi_{-j}(x) dx \\ &= \frac{i}{4\sqrt{\pi\tilde{c}}} \frac{1}{\beta_{j_1}} \left(\int_0^{\tilde{c}} e^{i(\beta_{j_1} - j_2 \pi / \tilde{c})x_2} \mathcal{X}(x_2) dx_2 + \int_0^{\tilde{c}} e^{i(\beta_{j_1} + j_2 \pi / \tilde{c})x_2} \mathcal{X}(x_2) dx_2 \right) \end{aligned}$$

If $\beta_{j_1} \neq \pm j_2 \pi / \tilde{c}$, then by integration by parts we have

$$\begin{aligned} \hat{K}_j &= \frac{1}{2\sqrt{\pi\tilde{c}}} \left[\frac{1}{(\alpha + j_1)^2 + (j_2 \pi / \tilde{c})^2 - k^2} + \frac{1}{2\beta_{j_1}(j_2 \pi / \tilde{c} - \beta_{j_1})} \int_0^{\tilde{c}} e^{i\beta_{j_1} x_2} \mathcal{X}'(x_2) e^{-i(j_2 \pi / \tilde{c})x_2} dx_2 \right. \\ &\quad \left. - \frac{1}{2\beta_{j_1}(j_2 \pi / \tilde{c} + \beta_{j_1})} \int_0^{\tilde{c}} e^{i\beta_{j_1} x_2} \mathcal{X}'(x_2) e^{i(j_2 \pi / \tilde{c})x_2} dx_2 \right] \end{aligned} \quad (2.2)$$

The last two integrals can be calculated by the one-dimensional Fast Fourier Transform (FFT) and matrix computation.

If $\beta_{j_1} = -j_2\pi/\tilde{c}$ with $j_2 \neq 0$ then we have

$$\hat{K}_j = \frac{i}{4\sqrt{\pi\tilde{c}}\beta_{j_1}} \int_0^{\tilde{c}} \mathcal{X}(x_2) dx_2 + \frac{1}{4\sqrt{\pi\tilde{c}}\beta_{j_1}(j_2\pi/\tilde{c} - \beta_{j_1})} \left[1 + \int_0^{\tilde{c}} \mathcal{X}'(x_2) e^{i(\beta_{j_1} - j_2\pi/\tilde{c})x_2} dx_2 \right]$$

The two integrals can be calculated by one-dimensional numerical quadratures. \hat{K}_j can be calculated similarly for the case $\beta_{j_1} = j_2\pi/\tilde{c}$ with $j_2 \neq 0$. Note that these two special cases seldom occurs; in fact, they can even be avoided by a perturbation of \tilde{c} . Therefore, we assume that these two special cases do not occur.

It should be noted that a direct evaluation of K by using the Fourier coefficients \hat{K}_j , that is, by the approximation $K_N = \sum_{j \in S_N} \hat{K}_j \phi_j$, will not lead to a convergent result due to the singularity at $x = 0$ of $K(x)$. In the next subsection we will introduce a convergent approximation to K with Fourier coefficients by removing the singularity of K .

2.2 Removal of the singularity

We now derive a convergent approximation to K with its Fourier coefficients by removing the singularity of K .

From the image representation (1.1), G is the sum of a singular function $(i/4)H_0^{(1)}(k|x|)$ and an analytic function $(i/4)\sum_{n \neq 0, n \in \mathbb{Z}} e^{i2\pi\alpha n} H_0^{(1)}(kr_n)$. Then the singularity at zero of $G(x)$ is the same as that of $(i/4)H_0^{(1)}(k|x|)$, so the singularity at zero of $K(x)$ is equivalent to that of $(i/4)H_0^{(1)}(k|x|)e^{-i\alpha x_1}$.

From the definition of the Hankel function:

$$H_0^{(1)}(k|x|) = J_0(k|x|) + iY_0(k|x|)$$

where the Bessel functions J_0 and Y_0 are defined by

$$\begin{aligned} J_0(k|x|) &= \sum_{m=0}^{+\infty} \frac{(-1)^m}{(m!)^2} \left(\frac{k|x|}{2}\right)^{2m} \\ Y_0(k|x|) &= \frac{2}{\pi} \ln \frac{k|x|}{2} J_0(k|x|) - \frac{1}{\pi} \sum_{m=0}^{\infty} \frac{(-1)^m}{(m!)^2} \left(\frac{k|x|}{2}\right)^{2m} \cdot 2\psi(m+1) \end{aligned}$$

with the digamma function ψ , we have the asymptotic behavior of $H_0^{(1)}(k|x|)$ at small $|x|$:

$$H_0^{(1)}(k|x|) = \frac{2i}{\pi} \ln |x| - \frac{2i}{\pi} \frac{k^2|x|^2}{4} \ln |x| + O(|x|^4 \ln |x|)$$

Thus, $K(x)$ has the asymptotic behavior at small $|x|$:

$$\begin{aligned} K(x) &\sim \frac{i}{4} H_0^{(1)}(k|x|) \cdot e^{-i\alpha x_1} \\ &= \left[-\frac{1}{2\pi} \ln |x| + \frac{1}{2\pi} \frac{k^2|x|^2}{4} \ln |x| + O(|x|^4 \ln |x|) \right] [1 - i\alpha x_1 + O(x_1^2)] \\ &= -\frac{1}{2\pi} \ln |x| + \frac{1}{2\pi} i\alpha x_1 \ln |x| + O(|x|^2 \ln |x|), \quad |x| \sim 0 \end{aligned} \tag{2.3}$$

Let $\mathcal{Y}_\varepsilon(t)$ be a smooth function for $t \geq 0$ such that $\mathcal{Y}_\varepsilon(t) = 1$ for $t \in [0, \varepsilon]$ and $\mathcal{Y}_\varepsilon(t) = 0$ for $t \in [2\varepsilon, \infty)$, where $0 < \varepsilon \ll 1$. Set

$$f_1 = -\frac{1}{2\pi} \ln|x| \cdot \mathcal{Y}_\varepsilon(|x|), \quad f_2 = -\frac{1}{2\pi} x_1 \ln|x| \cdot \mathcal{Y}_\varepsilon(|x|)$$

Then f_1, f_2 are known functions independent of k and α . Extend these two functions into bi-periodic functions in \mathbb{R}^2 with the same period as K and let $L = K - f_1 + i\alpha f_2$. Then L is a C^μ function with $0 < \mu < 2$.

The Fourier coefficients of L are given by

$$\hat{L}_j = \hat{K}_j - \hat{F}_{1,j} + i\alpha \hat{F}_{2,j} \quad (2.4)$$

where $\hat{F}_{1,j}$ and $\hat{F}_{2,j}$ are the Fourier coefficients of f_1 and f_2 , respectively. By a direct calculation it can be obtained that

$$\hat{F}_{1,j} = \frac{1}{j_1^2 + j_2^2 \pi^2 \tilde{c}^{-2}} \left(\frac{1}{2\sqrt{\pi\tilde{c}}} + \frac{1}{2\pi} \hat{\Phi}_{1,j} \right) \quad (2.5)$$

$$\hat{F}_{2,j} = \frac{1}{j_1^2 + j_2^2 \pi^2 \tilde{c}^{-2}} \left(-2ij_1 \hat{F}_{1,j} + \frac{1}{2\pi} \hat{\Phi}_{2,j} \right) \quad (2.6)$$

when $|j| \neq 0$, and

$$\begin{aligned} \hat{F}_{1,0} &= -\frac{1}{2\sqrt{\pi\tilde{c}}} \int_0^{2\varepsilon} t \ln(t) \mathcal{Y}_\varepsilon(t) dt \\ \hat{F}_{2,0} &= 0 \end{aligned}$$

Here, $\hat{\Phi}_{1,j}$ and $\hat{\Phi}_{2,j}$ are the Fourier coefficients of $\Phi_1(x) = (2 + \ln|x|) \mathcal{Y}'_\varepsilon(|x|)/|x| + \mathcal{Y}''_\varepsilon(|x|) \ln|x|$ and $\Phi_2(x) = x_1 \Phi_1(x)$, respectively. Note that Φ_1 and Φ_2 are smooth functions so their Fourier coefficients can be computed directly by 2D FFT.

Let

$$L_N(x) = \sum_{j \in S_N} \hat{L}_j \phi_j(x)$$

Then the values of L_N at the grid points can be efficiently computed by the 2D inverse FFT (IFFT).

Remark 2.1. Note that the functions Φ_1 and Φ_2 are independent of k and α , thus $\hat{F}_{1,j}$ and $\hat{F}_{2,j}$ can be assumed known for different k 's and α 's.

2.3 Evaluation of the Green's function at arbitrary points

We now have the values of L_N at the grid points. For an arbitrary point $x \in D_c$, we use the 2D interpolation to compute the value of $K(x)$ or $G(x)$. There are many 2D interpolation methods such as nearest-neighbor interpolation, bilinear interpolation, spline interpolation and bicubic interpolation. In this paper, we will use the bicubic interpolation, which only needs to solve a system of linear equations of 16 unknowns. The interpolation error is $O(h^4)$, where $h = O(N^{-1})$ is the largest grid size.

Algorithm 2.1. *Evaluation of the Green's function G . From Remark 2.1, $\hat{F}_{1,j}$ and $\hat{F}_{2,j}$ are pre-computed, saved and loaded.*

1. Preparation.

- (a) Calculate the Fourier coefficients \hat{K}_j by (2.2).
- (b) Calculate the Fourier coefficients \hat{L}_j by (2.4)
- (c) Calculate the values of L_N at the grid points by 2D IFFT.

2. Calculation.

- (a) Input a point x .
- (b) Check the size of $|x_2|$;
 - if $|x_2| > c$, use the series expansion (1.2);
 - if $|x_2| \leq c$, go to (c).
- (c) Find the unique real number $t \in [-\pi, \pi)$ and the unique integer n such that $x_1 = 2n\pi + t$.
- (d) Calculate the value of L_N at the point (t, x_2) by bicubic interpolation with the nearest 16 points. Then calculate the approximate value of $K(t, x_2)$ via $K_N(t, x_2) = L_N(t, x_2) + (f_1 - i\alpha f_2)(t, x_2)$.
- (e) Calculate the approximate value of $G(x)$ with $G_N(x) = e^{i\alpha x_1} K_N(t, x_2)$.

It is seen that in Algorithm 2.1, the preparation step is the most time-consuming one, but it only needs to run once. This step involves the calculation of the Fourier coefficients \hat{K}_j and 2D IFFT. The evaluation of the Fourier coefficients \hat{K}_j can be carried out by 1D FFT and matrix calculation, which is of high efficiency in MATLAB. The details will be explained in Section 6.

2.4 Derivatives of the Green function

In the integral equation method for solving scattering problems by periodic structures, we also need to evaluate the first- and second-order derivatives of the quasi-periodic Green's function. In this subsection, we briefly discuss extension of the above idea to their efficient and accurate computation.

2.4.1 First-order derivatives

By the definition of K (see Subsection 2.1) it follows that $G(x) = \exp(i\alpha x_1)K(x)$ for all $x \in D_c$. Then we have

$$\frac{\partial G(x)}{\partial x_1} = i\alpha e^{i\alpha x_1} K(x) + e^{i\alpha x_1} \frac{\partial K(x)}{\partial x_1}, \quad \frac{\partial G(x)}{\partial x_2} = e^{i\alpha x_1} \frac{\partial K(x)}{\partial x_2}$$

Define

$$K_1(x) = i\alpha K(x) + \frac{\partial K(x)}{\partial x_1}, \quad K_2(x) = \frac{\partial K(x)}{\partial x_2}$$

Then $K_1(x) = \exp(-i\alpha x_1) \partial G(x) / \partial x_1$, $K_2(x) = \exp(-i\alpha x_1) \partial G(x) / \partial x_2$ for all $x \in D_c$. The functions K_1 and K_2 are bi-periodic with the same periods as K . Denote by $\hat{K}_{1,j}$ and $\hat{K}_{2,j}$ the

Fourier coefficients of K_1 and K_2 , respectively. Then $\hat{K}_{1,j} = i(\alpha + j_1)\hat{K}_j$ and $\hat{K}_{2,j} = ij_2(\pi/\tilde{c})\hat{K}_j$. We now remove the singularity of K_1 and K_2 . The singularity at zero of K_1 is given by

$$\begin{aligned} K_1(x) &\sim e^{-i\alpha x_1} \frac{i}{4} \frac{\partial H_0^{(1)}(k|x|)}{\partial x_1} = -\frac{ik}{4} e^{-i\alpha x_1} H_1^1(k|x|) \frac{x_1}{|x|} \\ &= -\frac{ik}{4} \left(1 - i\alpha x_1 - \frac{\alpha^2}{2} x_1^2 + O(x_1^3) \right) \left(\frac{ik}{\pi} x_1 \ln |x| - \frac{2i}{\pi} \frac{x_1}{k|x|^2} + O(|x|^2 \ln |x|) \right) \\ &= -\frac{1}{2\pi} \left(-\frac{k^2}{2} x_1 \ln |x| + \frac{x_1}{|x|^2} - i\alpha \frac{x_1^2}{|x|^2} - \frac{\alpha^2}{2} \frac{x_1^3}{|x|^2} \right) + O(|x|^2 \ln |x|) \end{aligned}$$

Define the singular function

$$h_1(x) = -\frac{1}{2\pi} \left(-\frac{k^2}{2} x_1 \ln |x| + \frac{x_1}{|x|^2} - i\alpha \frac{x_1^2}{|x|^2} - \frac{\alpha^2}{2} \frac{x_1^3}{|x|^2} \right) \mathcal{Y}_\varepsilon(|x|),$$

where \mathcal{Y}_ε is defined in Subsection 2.2. Then $K_1(x) = [K_1(x) - h_1(x)] + h_1(x)$ where the function $K_1(x) - h_1(x)$ has a better regularity. The Fourier coefficients $\hat{H}_{1,j}$ of h_1 can be calculated directly, similarly as for $\hat{F}_{1,j}$ and $\hat{F}_{2,j}$ in Subsection 2.2. Then the function $K_1 - h_1$ can be accurately evaluated efficiently at the grid points via the 2D IFFT by using the known Fourier coefficients $\hat{K}_{1,j} - \hat{H}_{1,j}$. Finally, the function K_1 or $\partial G(x)/\partial x_1$ can be accurately evaluated efficiently at an arbitrary point $x \in D_c$ by bi-cubic interpolation.

Similarly, the function K_2 or $\partial G(x)/\partial x_2$ can also be accurately evaluated efficiently. In this case, the function $K_2(x) = [K_2(x) - h_2(x)] + h_2(x)$ with a regular function $K_2(x) - h_2(x)$, where the singular function

$$h_2(x) = -\frac{1}{2\pi} \left(-\frac{k^2}{2} x_2 \ln |x| + \frac{x_2}{|x|^2} - i\alpha \frac{x_1 x_2}{|x|^2} - \frac{\alpha^2}{2} \frac{x_1^2 x_2}{|x|^2} \right) \mathcal{Y}_\varepsilon(|x|).$$

2.4.2 Second-order derivatives

The second-order derivatives of G usually occurs in the hyper-singular integral operator T defined by

$$(T\phi)(x) = \frac{\partial}{\partial \nu(x)} \int_{\Gamma} \frac{\partial G}{\partial \nu(y)}(x, y) \phi(y) ds(y)$$

for ϕ in certain space, where $\nu(x)$ is the unit normal vector at $x \in \Gamma$. In the integral equation methods for wave scattering from periodic structures, we usually need to compute the difference between two T operators with different wave numbers. Thus, we will discuss the accurate and efficient evaluation of the differences of second-order derivatives of G_{k_1} and G_{k_2} for different wave numbers k_1 and k_2 rather than the second-order derivatives of G itself, where G_{k_j} is defined similarly as G with k replaced by k_j , $j = 1, 2$.

The second-order derivatives of G in D_c can be calculated as follows:

$$\begin{aligned} \frac{\partial^2 G(x)}{\partial x_1^2} &= -\alpha^2 e^{i\alpha x_1} K(x) + 2i\alpha e^{i\alpha x_1} \frac{\partial K(x)}{\partial x_1} + e^{i\alpha x_1} \frac{\partial^2 K(x)}{\partial x_1^2} \\ \frac{\partial^2 G(x)}{\partial x_1 \partial x_2} &= i\alpha e^{i\alpha x_1} \frac{\partial K}{\partial x_2} + e^{i\alpha x_1} \frac{\partial^2 K(x)}{\partial x_1 \partial x_2} \\ \frac{\partial^2 G(x)}{\partial x_2 \partial x_1} &= e^{i\alpha x_1} \frac{\partial^2 K(x)}{\partial x_2^2} \end{aligned}$$

Define

$$\begin{aligned} K_{11}(x) &= -\alpha^2 K(x) + 2i\alpha \frac{\partial K(x)}{\partial x_1} + \frac{\partial^2 K(x)}{\partial x_1^2} \\ K_{12}(x) &= i\alpha \frac{\partial K}{\partial x_2} + \frac{\partial^2 K(x)}{\partial x_1 \partial x_2} \\ K_{22}(x) &= \frac{\partial^2 K(x)}{\partial x_2^2} \end{aligned}$$

Then $K_{11}(x) = \exp(-i\alpha x_1) \partial^2 G(x) / \partial x_1^2$, $K_{12}(x) = \exp(-i\alpha x_1) \partial^2 G(x) / \partial x_1 \partial x_2$ and $K_{22}(x) = \exp(-i\alpha x_1) \partial^2 G(x) / \partial x_2^2$ in D_c , which are bi-periodic. Their Fourier coefficients are given as $\hat{K}_{11,j} = -(\alpha + j_1)^2 \hat{K}_j$, $\hat{K}_{12,j} = -(\alpha + j_1) j_2 (\pi/\tilde{c}) \hat{K}_j$ and $\hat{K}_{22,j} = -(j_2 \pi/\tilde{c})^2 \hat{K}_j$. When $|x| \rightarrow 0$, we have

$$\begin{aligned} K_{11}(x) &\sim e^{-i\alpha x_1} \frac{\partial^2 G(x)}{\partial x_1^2} \sim \frac{i}{4} e^{-i\alpha x_1} \frac{\partial^2 H_0^{(1)}(k|x|)}{\partial x_1^2} \\ &= \frac{ik}{4} e^{-i\alpha x_1} \left[H_1^{(1)}(k|x|) \frac{|x|^2 - x_1^2}{|x|^3} + \frac{kx_1^2}{2|x|^2} [H_0^{(1)}(k|x|) - H_2^{(1)}(k|x|)] \right] \\ &= \frac{k^2}{2\pi} e^{-i\alpha x_1} \left(\frac{1}{2} \ln |x| + \frac{x_1^2}{2|x|^2} \right) + \frac{e^{-i\alpha x_1}}{\pi} \left(\frac{1}{|x|^2} - \frac{2x_1^2}{|x|^4} \right) + O(|x|^2 \ln |x|) \end{aligned}$$

Let $T_{11}(x) = K_{k_1,11}(x) - K_{k_2,11}(x)$, where $K_{k_j,11}$ is defined similarly as K_{11} with k replaced by k_j , $j = 1, 2$. Then the asymptotic behavior of T_{11} at $x = 0$ is

$$\begin{aligned} T_{11}(x) &\sim \frac{k_1^2 - k_2^2}{2\pi} e^{-i\alpha x_1} \left(\frac{1}{2} \ln |x| + \frac{x_1^2}{2|x|^2} + O(|x|^2 \ln |x|) \right) \\ &= -\frac{k_1^2 - k_2^2}{2\pi} \left(\frac{1}{2} \ln |x| - \frac{i}{2} \alpha x_1 \ln |x| + \frac{x_1^2}{2|x|^2} - \frac{i\alpha x_1^3}{2|x|^2} \right) + O(|x|^2 \ln |x|) \end{aligned}$$

Define

$$h_{11}(x) = -\frac{k_1^2 - k_2^2}{2\pi} \left(\frac{1}{2} \ln |x| - \frac{i}{2} \alpha x_1 \ln |x| + \frac{x_1^2}{2|x|^2} - \frac{i\alpha x_1^3}{2|x|^2} \right) \mathcal{Y}_\varepsilon(|x|)$$

Then $T_{11} = (T_{11} - h_{11}) + h_{11}$ with a regular function $T_{11} - h_{11}$. The Fourier coefficients \hat{H}_{11} of h_{11} can be calculated directly as in Subsection 2.2 (cf. (2.5) and (2.6)), and the Fourier coefficients of $T_{11} - h_{11}$ are given as $\hat{T}_{11} - \hat{H}_{11} = \hat{K}_{11,j}^{(k_1)} - \hat{K}_{11,j}^{(k_2)} - \hat{H}_{11}$, where $\hat{K}_{11,j}^{(k_i)}$ is the same as $\hat{K}_{11,j}$ with k replaced by k_i ($i = 1, 2$).

The regular function $T_{11} - h_{11}$ can be accurately evaluated efficiently at the grid points via the 2D IFFT, by using the known Fourier coefficients $\hat{T}_{11} - \hat{H}_{11}$. Then at an arbitrary point $x \in D_c$ the function $T_{11}(x) - h_{11}(x)$ can be evaluated efficiently and accurately by bi-cubic interpolation. Thus, the function $T_{11}(x)$ can be computed efficiently and accurately at an arbitrary point $x \in D_c$ by bi-cubic interpolation since $T_{11}(x) = [T_{11}(x) - h_{11}(x)] + h_{11}(x)$. Similarly as before, it can be shown that this computation method is of second-order convergence with the error bound $C|k_1^4 - k_2^4|/N^2$ since the leading term of the Fourier coefficients $\hat{T}_{11} - \hat{H}_{11}$ is

$$\hat{T}_{11} - \hat{H}_{11} \sim \frac{k_1^4 - k_2^4}{[(\alpha + j_1)^2 + (j_2 \pi/\tilde{c})^2 - k_1^2][(\alpha + j_1)^2 + (j_2 \pi/\tilde{c})^2 - k_2^2]}$$

for large j_1, j_2 .

The functions $T_{12} = K_{k_1,12} - K_{k_2,12}$ and $T_{22} = K_{k_1,22} - K_{k_2,22}$ can be evaluated similarly since $T_{12} = (T_{12} - h_{12}) + h_{12}$ and $T_{22} = (T_{22} - h_{22}) + h_{22}$ with regular functions $T_{12} - h_{12}$ and $T_{22} - h_{22}$ and singular functions

$$\begin{aligned} h_{12}(x) &= -\frac{k_1^2 - k_2^2}{2\pi} \left(\frac{x_1 x_2}{2|x|^2} - \frac{i\alpha}{2} \frac{x_1^2 x_2}{|x|^2} \right) \mathcal{Y}_\varepsilon(|x|) \\ h_{22}(x) &= -\frac{k_1^2 - k_2^2}{2\pi} \left(\frac{1}{2} \ln|x| - \frac{1}{2} i\alpha x_1 \ln|x| + \frac{x_2^2}{2|x|^2} - \frac{i\alpha}{2} \frac{x_1 x_2^2}{|x|^2} \right) \mathcal{Y}_\varepsilon(|x|) \end{aligned}$$

Here, $K_{k_j,12}$ and $K_{k_j,22}$ are defined similarly as K_{12} and K_{22} , respectively, with k replaced by k_j , $j = 1, 2$.

3 The FFT-based algorithm in three dimensions

3.1 Periodization and Fourier coefficients

Set $D_{dc} = [-\pi, \pi] \times [-\pi, \pi] \times [-c, c]$, where c is a chosen positive constant such that for $|x_3| \geq c$ the series representation (1.3) can be directly used to evaluate G_d efficiently and accurately. Thus, we only consider the case when $x \in D_{dc}$.

By (1.3) we know that

$$e^{-i\alpha_1 x_1 - i\alpha_2 x_2} G_d(x) = \frac{i}{8\pi^2} \sum_{n_1, n_2 \in \mathbb{Z}} \frac{1}{\beta_{n_1, n_2}} e^{in_1 x_1 + in_2 x_2 + i\beta_{n_1, n_2} |x_3|}$$

which is periodic in both x_1 and x_2 with period 2π . Now choose $\tilde{c} > c$ and set $D_{d\tilde{c}} = [-\pi, \pi] \times [-\pi, \pi] \times [-\tilde{c}, \tilde{c}]$. Define

$$K_d(x) = e^{-i\alpha_1 x_1 - i\alpha_2 x_2} G_d(x) \mathcal{X}(|x_3|) \quad \text{for } x \in D_{d\tilde{c}}$$

and extend it into a periodic function in \mathbb{R}^3 , denoted by K_d again. Note that K_d is smooth in $D_{d\tilde{c}} \setminus \{0\}$ and

$$G_d(x) = e^{i\alpha_1 x_1 + i\alpha_2 x_2} K_d(x) \quad \text{for } x \in D_{dc}. \quad (3.1)$$

We now calculate the Fourier coefficients of $K_d(x)$. For a large integer $N > 0$ divide $D_{d\tilde{c}}$ into $2N \times 2N \times 2N$ uniform grids. Set $S_N = \{l = (l_1, l_2, l_3) \in \mathbb{Z}^3 : -N \leq l_1, l_2, l_3 < N\}$. For $j = (j_1, j_2, j_3) \in S_N$ denote by $x_j = (x_{1,j_1}, x_{2,j_2}, x_{3,j_3})$ the grid points, where $x_{1,j_1} = j_1\pi/N$, $x_{2,j_2} = j_2\pi/N$, $x_{3,j_3} = j_3\tilde{c}/N$. Let

$$\phi_j(x) = \frac{1}{\sqrt{8\pi^2 \tilde{c}}} \exp[i(j_1 x_1 + j_2 x_2 + j_3 x_3/\tilde{c})], \quad j = (j_1, j_2, j_3) \in \mathbb{Z}^3.$$

Then $\{\phi_j\}_{j \in \mathbb{Z}^3}$ is the Fourier basis of $L^2(D_{d\tilde{c}})$ and the Fourier series of K_d is given as $K_d(x) = \sum_{j \in \mathbb{Z}^3} \hat{K}_{dj} \phi_j(x)$, where \hat{K}_{dj} is the j -th Fourier coefficient of K_d given by

$$\begin{aligned} \hat{K}_{dj} &= \int_{D_{d\tilde{c}}} K_d(x) \phi_{-j}(x) dx = \int_{D_{d\tilde{c}}} e^{-i\alpha_1 x_1 - i\alpha_2 x_2} G_d(x) \mathcal{X}(|x_3|) \phi_{-j}(x) dx \\ &= \frac{1}{\sqrt{8\pi^2 \tilde{c}}} \frac{i}{8\pi^2} \int_{D_{d\tilde{c}}} \sum_{n_1, n_2 \in \mathbb{Z}} \frac{1}{\beta_{n_1, n_2}} e^{in_1 x_1 + in_2 x_2 + i\beta_{n_1, n_2} |x_3|} \mathcal{X}(|x_3|) e^{-ij_1 x_1 - ij_2 x_2 - ij_3 x_3/\tilde{c}} dx \\ &= \frac{i}{2\sqrt{8\pi^2 \tilde{c}}} \frac{1}{\beta_{j_1, j_2}} \int_0^{\tilde{c}} \left[e^{i(\beta_{j_1, j_2} - j_3/\tilde{c}) x_3} + e^{-i(\beta_{j_1, j_2} - j_3/\tilde{c}) x_3} \right] \mathcal{X}(x_3) dx_3 \end{aligned} \quad (3.2)$$

If $\beta_{j_1,j_2} \neq \pm j_3\pi/\tilde{c}$ it then follows by integration by parts that

$$\begin{aligned}\hat{K}_{dj} &= \frac{1}{\sqrt{8\pi^2\tilde{c}}}\left[\frac{1}{(\alpha_1+j_1)^2 + (\alpha_2+j_2)^2 + (j_3\pi/\tilde{c})^2 - k^2}\right. \\ &\quad + \frac{1}{2\beta_{j_1,j_2}(j_3\pi/\tilde{c} - \beta_{j_1,j_2})}\int_0^{\tilde{c}} e^{i(\beta_{j_1,j_2} - j_3\pi/\tilde{c})x_3} \mathcal{X}'(x_3) dx_3 \quad (3.3) \\ &\quad \left. - \frac{1}{2\beta_{j_1,j_2}(j_3\pi/\tilde{c} + \beta_{j_1,j_2})}\int_0^{\tilde{c}} e^{i(\beta_{j_1,j_2} + j_3\pi/\tilde{c})x_3} \mathcal{X}'(x_3) dx_3\right] \quad (3.4)\end{aligned}$$

The two integrals can be calculated efficiently by 1D FFT.

If $\beta_{j_1,j_2} = -j_3\pi/\tilde{c}$ we have

$$\begin{aligned}\hat{K}_{dj} &= \frac{i}{2\sqrt{8\pi^2\tilde{c}}\beta_{j_1,j_2}}\int_0^{\tilde{c}} \mathcal{X}(x_3) dx_3 \\ &\quad + \frac{1}{2\sqrt{8\pi^2\tilde{c}}\beta_{j_1,j_2}(j_3\pi/\tilde{c} - \beta_{j_1,j_2})}\left(1 + \int_0^{\tilde{c}} \mathcal{X}'(x_3) e^{i(\beta_{j_1,j_2} - ij_3\pi/\tilde{c})x_3} dx_3\right) \quad (3.5)\end{aligned}$$

The two integrals can be calculated by 1D FFT or 1D numerical quadratures. The case with $\beta_{j_1,j_2} = j_3\pi/\tilde{c}$ can be dealt with similarly. Note that these cases can be avoided by choosing \tilde{c} properly, thus we assume that these cases don't occur in this paper.

Similar to the 2D case, the direct evaluation of K_d by using the Fourier coefficients $K_{dN}(x) = \sum_{j \in S_N} \hat{K}_{dj} \phi_j(x)$ for $x \in D_{dc}$, will not lead to a convergent result, due to the singularity at $x = 0$ of K_d . In the next subsection we will introduce a convergent approximation to K_d by removing the singularity of K_d .

3.2 Removal of the singularity

Since $G_d(x)$ can be written as $G_d(x) = \exp(ik|x|)(4\pi|x|)^{-1} + a(x)$ in the neighborhood of $x = 0$, where a is an analytic function, then the singularity of $K_d(x)$ at $x = 0$ is the same as $\exp[-i(\alpha_1 x_1 + \alpha_2 x_2)] \exp(ik|x|)(4\pi|x|)^{-1}$. Define

$$F(x) = e^{-i\alpha_1 x_1 - i\alpha_2 x_2} \frac{e^{ik|x|}}{4\pi|x|} \mathcal{Y}_\varepsilon(|x|), \quad x \in D_{d\tilde{c}}$$

for some positive number $\varepsilon \ll \min\{1, \tilde{c}\}/2$. Then F is zero outside of $D_{d\tilde{c}}$ and can be extended into a periodic function in \mathbb{R}^3 , denoted by F again, with the same period as K_d . Thus, $L_d(x) := K_d(x) - F(x)$ is smooth in $D_{d\tilde{c}}$ and periodic in \mathbb{R}^3 . The j -th Fourier coefficient of L_d is given as $\hat{L}_{dj} = \hat{K}_{dj} - \hat{F}_j$, where \hat{K}_{dj} and \hat{F}_j are the j -th Fourier coefficients of K_d and F , respectively. By a similar argument as in [27] it can be derived that

$$\begin{aligned}\hat{F}_j &= \frac{1}{\sqrt{8\pi^2\tilde{c}}} \frac{1}{(\alpha_1+j_1)^2 + (\alpha_2+j_2)^2 + (j_3\pi/\tilde{c})^2 - k^2} \\ &\quad \cdot \left[1 - \int_{D_{d\tilde{c}}} \frac{e^{ik|x|}}{4\pi|x|} [2ik\mathcal{Y}'_\varepsilon(|x|) + \mathcal{Y}''_\varepsilon(|x|)] e^{-i(\alpha_1,j_1 x_1 + \alpha_2,j_2 x_2 + j_3 x_3 \pi/\tilde{c})} dx\right] \quad (3.6)\end{aligned}$$

The integral can be calculated efficiently with 3D FFT.

Define the truncated Fourier series

$$L_{dN}(x) = \sum_{j \in S_N} \hat{L}_{dj} \phi_j(x). \quad (3.7)$$

Then L_{dN} converges to L with the convergence rate $O(N^{-m})$ for any $m \in \mathbb{N}^+$, as $N \rightarrow \infty$ (see Theorem 5.4 in Section 5). The values of L_{dN} on the grid points can be evaluated efficiently by 3D IFFT.

3.3 Evaluation of the Green function at arbitrary points

The value of $L_{dN}(x)$ at an arbitrary point x can be computed from the values of L_{dN} at the grid points by using tricubic interpolation (e.g., the algorithm discussed in [13]). The relative error of the tricubic interpolation is h^4 , where $h = O(1/N)$ is the largest grid size. Thus, for an arbitrary point $x \in D_{dc}$ the function $K_d(x)$ or the Green function $G_d(x)$ can be evaluated efficiently and accurately since $K_d(x) = L_d(x) + F(x)$. This is summarized in the following algorithm.

Algorithm 3.1. *The evaluation of the Green function $G_d(x)$.*

1. Preparation

- (a) Calculate the coefficients \hat{K}_{dj} by (3.2)-(3.5).
- (b) Calculate the coefficients \hat{L}_{dj} via the formula $\hat{L}_{dj} = \hat{K}_{dj} - \hat{F}_j$ and (3.6).
- (c) Calculate the values of L_{dN} on the grid points by 3D IFFT.

2. Calculation

- (a) Input a point x .
- (b) Check the size of $|x_3|$;
 - if $|x_3| > c$, use (1.3) to calculate the value $G_d(x)$;
 - if $|x_3| \leq c$, go to (c).
- (c) Find the unique real numbers $t_1, t_2 \in [-\pi, \pi)$ and integers n_1, n_2 such that $x_1 = 2n_1\pi + t_1$, $x_2 = 2n_2\pi + t_2$.
- (d) Calculate the value $L_{dN}(t_1, t_2, x_3)$ by tri-cubic interpolation.
- (e) Calculate the approximate value of $K_d(t_1, t_2, x_3)$ via $K_{dN}(t_1, t_2, x_3) = L_{dN}(t_1, t_2, x_3) + F(t_1, t_2, x_3)$.
- (f) Calculate the approximate value of $G_d(t_1, t_2, x_3)$ by the formula $G_{dN}(t_1, t_2, x_3) = e^{i\alpha_1 t_1 + i\alpha_2 t_2} K_{dN}(t_1, t_2, x_3)$.

In this algorithm, the preparation step is the most time-consuming one; however, it needs to run only once. The calculation step mainly needs to compute a multiplication of a 64×64 matrix with a 64-dimensional vector and therefore consumes very little time. The details will be discussed in Section 6.

4 The FFT-based algorithm in the Maxwell case

The doubly quasi-periodic Green's tensor $\mathbb{G}(x)$ for Maxwell's equations in 3D can be rewritten in the form

$$\mathbb{G}(x) = G_d(x)\mathbb{I} + \frac{1}{k^2} \begin{pmatrix} \frac{\partial^2 G_d}{\partial x_1^2} & \frac{\partial^2 G_d}{\partial x_1 \partial x_2} & \frac{\partial^2 G_d}{\partial x_1 \partial x_3} \\ \frac{\partial^2 G_d}{\partial x_2 \partial x_1} & \frac{\partial^2 G_d}{\partial x_2^2} & \frac{\partial^2 G_d}{\partial x_2 \partial x_3} \\ \frac{\partial^2 G_d}{\partial x_3 \partial x_1} & \frac{\partial^2 G_d}{\partial x_3 \partial x_2} & \frac{\partial^2 G_d}{\partial x_3^2} \end{pmatrix} \quad (4.1)$$

Besides the values of the 3D Green's function $G_d(x)$, we only need to evaluate the second-order derivatives $\partial^2 G_d / (\partial x_p \partial x_q)$, $p, q = 1, 2, 3$. Define

$$K^{pq}(x) = e^{-i\alpha_1 x_1 - i\alpha_2 x_2} \frac{\partial^2}{\partial x_p \partial x_q} [G_d(x) \mathcal{X}(|x_3|)]$$

Then

$$\frac{\partial^2 G_d(x)}{\partial x_p \partial x_q} = e^{i\alpha_1 x_1 + i\alpha_2 x_2} K^{pq}(x), \quad x \in D_c \quad (4.2)$$

From the definition of K_d it follows that

$$\begin{aligned} K^{pq} &= e^{-i\alpha_1 x_1 - i\alpha_2 x_2} \frac{\partial^2}{\partial x_p \partial x_q} [e^{i\alpha_1 x_1 + i\alpha_2 x_2} K_d(x)] \\ &= e^{-i\alpha_1 x_1 - i\alpha_2 x_2} \frac{\partial^2}{\partial x_p \partial x_q} \left[e^{i\alpha_1 x_1 + i\alpha_2 x_2} \sum_{j \in \mathbb{Z}^3} \hat{K}_{dj} \phi_j(x) \right] \\ &= \frac{1}{\sqrt{8\pi^2 \tilde{c}}} e^{-i\alpha_1 x_1 - i\alpha_2 x_2} \frac{\partial^2}{\partial x_p \partial x_q} \sum_{j \in \mathbb{Z}^3} \hat{K}_{dj} e^{i\alpha_{1,j_1} x_1 + i\alpha_{2,j_2} x_2 + i j_3 x_3 \pi / \tilde{c}} \end{aligned}$$

Set $c_j^1 = \alpha_{1,j_1}$, $c_j^2 = \alpha_{2,j_2}$, $c_j^3 = j_3 \pi / \tilde{c}$. Then, by a direct calculation the Fourier coefficients of K^{pq} are given as $\hat{K}_j^{pq} = -c_j^p c_j^q \hat{K}_{dj}$.

As the Helmholtz case, we also need to remove the singularity of K^{pq} . For $x \in D_{d\tilde{c}}$ let

$$\begin{aligned} F^{pq}(x) &= e^{-i\alpha_1 x_1 - i\alpha_2 x_2} \frac{\partial^2}{\partial x_p \partial x_q} [e^{i\alpha_1 x_1 + i\alpha_2 x_2} F(x)], \\ L_d^{pq}(x) &= e^{-i\alpha_1 x_1 - i\alpha_2 x_2} \frac{\partial^2}{\partial x_p \partial x_q} [e^{i\alpha_1 x_1 + i\alpha_2 x_2} L_d(x)], \end{aligned}$$

where F and L_d are defined in Section 3 and satisfy that $L_d(x) = K_d(x) - F(x)$ is smooth in $D_{d\tilde{c}}$ and periodic in \mathbb{R}^3 . Then $L_d^{pq}(x) = K_d^{pq}(x) - F^{pq}(x)$ is also smooth in $D_{d\tilde{c}}$ and periodic in \mathbb{R}^3 , and the Fourier coefficients of F^{pq} and L^{pq} are given, respectively, as $\hat{F}_j^{pq} = -c_j^p c_j^q \hat{F}_j$ and $\hat{L}_{dj}^{pq} = -c_j^p c_j^q \hat{L}_{dj}$.

With these Fourier coefficients, the values of the truncated Fourier series $L_{dN}^{pq}(x) = \sum_{j \in S_N} \hat{L}_{dj}^{pq} \phi_j(x)$ at the grid points can be efficiently evaluated by 3D IFFT. From these values of

$L_{dN}^{pq}(x)$ at the grid points, and by tricubic interpolation the value $L_{dN}^{pq}(x)$ at an arbitrary point $x \in D_{dc}$ can be efficiently computed. Finally, for an arbitrary point $x \in D_{dc}$ the approximate value of $K^{pq}(x)$ (via the formula $K_{dN}^{pq}(x) := L_{dN}^{pq}(x) + F^{pq}(x)$) and therefore $\partial^2 G_d(x)/(\partial x_p \partial x_q)$ (via (4.2)) can be efficiently obtained.

Based on the above idea and Algorithm 3.1, the following algorithm is given to evaluate the Green function $\mathbb{G}(x)$ efficiently and accurately.

Algorithm 4.1. *Evaluation of the Green function $\mathbb{G}(x)$.*

1. Preparation

- (a) Calculate the coefficients \hat{K}_{dj} by (3.2)-(3.5).
- (b) Calculate the coefficients \hat{L}_{dj} via the formula $\hat{L}_{dj} = \hat{K}_{dj} - \hat{F}_j$ and (3.6).
- (c) Calculate the coefficients \hat{L}_{dj}^{pq} via the formula $\hat{L}_{dj}^{pq} = -c_j^p c_j^q \hat{L}_{dj}$.
- (d) Calculate the values of L_{dN} and L_{dN}^{pq} at the grid points by 3D IFFT.

2. Calculation

- (a) Input a point x .
- (b) Check the size of $|x_3|$;
 - if $|x_3| > c$, use (1.3) and its derivatives to calculate the value $\mathbb{G}(x)$;
 - if $|x_3| \leq c$, go to (c).
- (c) Find the unique real numbers $t_1, t_2 \in [-\pi, \pi)$ and integers n_1, n_2 such that $x_1 = 2n_1\pi + t_1$, $x_2 = 2n_2\pi + t_2$.
- (d) Calculate the value $L_{dN}(t_1, t_2, x_3)$ and $L_{dN}^{pq}(t_1, t_2, x_3)$ by tri-cubic interpolation.
- (e) Calculate the approximate value of $K_d(t_1, t_2, x_3)$ via $K_{dN}(t_1, t_2, x_3) = L_{dN}(t_1, t_2, x_3) + F(t_1, t_2, x_3)$.
- (f) Calculate the approximate value of $K^{pq}(t_1, t_2, x_3)$ via $K_{dN}^{pq}(t_1, t_2, x_3) = L_{dN}^{pq}(t_1, t_2, x_3) + F^{pq}(t_1, t_2, x_3)$.
- (g) Calculate the approximate value of $G_d(t_1, t_2, x_3)$ by the formula $G_{dN}(t_1, t_2, x_3) = e^{i\alpha_1 t_1 + i\alpha_2 t_2} K_{dN}(t_1, t_2, x_3)$.
- (h) Calculate the approximate value of $\partial^2 G_d(t_1, t_2, x_3)/(\partial x_p \partial x_q)$ via the formula $\partial^2 G_{dN}(t_1, t_2, x_3)/(\partial x_p \partial x_q) = e^{i\alpha_1 t_1 + i\alpha_2 t_2} K_{dN}(t_1, t_2, x_3)$.
- (i) Calculate the approximate value of $\mathbb{G}(x)$ by (4.1).

Similar to Algorithm 3.1, in this algorithm, the most time-consuming step is also the preparation step, which only needs to run once. The calculation step consists mainly of seven interpolation processes and is very efficient.

5 Convergence analysis

In this section, we will study the convergence and error estimates of Algorithms 2.1, 3.1 and 4.1.

5.1 The two-dimensional case

Theorem 5.1. *For any wavenumber $k > 0$ and any positive integer N , L_N converges uniformly to L with second-order accuracy as $N \rightarrow \infty$, that is,*

$$\|L_N - L\|_{L^\infty(D_{\tilde{c}})} = O\left(\frac{k^2 + 1}{N^2}\right)$$

Proof. From (2.2), (2.5) and (2.6), the leading order of \hat{K}_j , $\hat{F}_{1,j}$ and $\hat{F}_{2,j}$ for $|j| \rightarrow \infty$ is:

$$\begin{aligned}\hat{K}_j &\sim \frac{1}{2\sqrt{\pi\tilde{c}}} \cdot \frac{1}{(\alpha + j_1)^2 + (j_2\pi/\tilde{c})^2 - k^2} \\ \hat{F}_{1,j} &\sim \frac{1}{2\sqrt{\pi\tilde{c}}} \cdot \frac{1}{j_1^2 + (j_2\pi/\tilde{c})^2} \\ \hat{F}_{2,j} &\sim -\frac{1}{\sqrt{\pi\tilde{c}}} \cdot \frac{ij_1}{(j_1^2 + (j_2\pi/\tilde{c})^2)^2}\end{aligned}$$

Then the leading order of \hat{L}_j is

$$\hat{L}_j = \hat{K}_j - \hat{F}_{1,j} + i\alpha\hat{F}_{2,j} \sim \frac{(k^2 - \alpha^2)(j_1^2 + (j_2\pi/\tilde{c})^2) + 4\alpha^2 j_1^2 + 2\alpha^3 j_1 - 2\alpha j_1 k^2}{2\sqrt{\pi\tilde{c}}((\alpha + j_1)^2 + (j_2\pi/\tilde{c})^2 - k^2)(j_1^2 + (j_2\pi/\tilde{c})^2)^2}$$

Thus, for any $x \in D_{\tilde{c}}$ we have

$$\begin{aligned}|L(x) - L_N(x)| &= \left| \sum_{j \notin S_N} \hat{L}_j \phi_j(x) \right| \leq \frac{1}{2\sqrt{\pi\tilde{c}}} \sum_{j \notin S_N} |\hat{L}_j| \\ &\sim \frac{1}{4\pi\tilde{c}} \sum_{j \notin S_N} \frac{|(k^2 - \alpha^2)(j_1^2 + (j_2\pi/\tilde{c})^2) + 4\alpha^2 j_1^2 + 2\alpha^3 j_1 - 2\alpha j_1 k^2|}{((\alpha + j_1)^2 + (j_2\pi/\tilde{c})^2 - k^2)(j_1^2 + (j_2\pi/\tilde{c})^2)^2} \\ &= O\left(\frac{k^2 + 1}{N^2}\right)\end{aligned}$$

The proof is completed. \square

Theorem 5.2. *For any $x \in D_c$ the error between the exact value $G(x)$ and the numerical value $\tilde{G}_N(x)$ obtained by Algorithm 2.1 satisfies the following estimate*

$$|G(x) - \tilde{G}_N(x)| \leq C\left(\frac{k^2 + 2}{N^2}\right)$$

where C is a constant independent of k and N .

Proof. By Theorem 5.1 we have that at any grid point x^*

$$|L(x^*) - L_N(x^*)| \leq C\left(\frac{k^2 + 1}{N^2}\right)$$

Note that the procedure of computing $L_N(x^*)$ makes use of FFT to compute the Fourier coefficients of L with the error bounded above by CN^{-2} . So the value we actually obtained is $\tilde{L}_N(x^*)$ with the Fourier coefficients $\hat{\tilde{L}}_j$ satisfying that $|\hat{L}_j - \hat{\tilde{L}}_j|/|\hat{L}_j| \leq CN^{-2}$. Thus we have

$$\begin{aligned}|L(x^*) - \tilde{L}_N(x^*)| &\leq |L(x^*) - L_N(x^*)| + |L_N(x^*) - \tilde{L}_N(x^*)| \\ &\leq C\left(\frac{k^2 + 1}{N^2}\right) + C\left(\frac{1}{N^2}\right) = C\left(\frac{k^2 + 2}{N^2}\right)\end{aligned}$$

For any $x \in D_c$ the value $\tilde{L}_N(x)$ is obtained by bi-cubic interpolation with the interpolation error $O(N^{-4})$. Then

$$|L(x) - \tilde{L}_N(x)| \leq C \frac{k^2 + 2}{N^2} (1 + O(N^{-4})) = C \frac{k^2 + 2}{N^2}$$

The required error estimate then follows from this since $\tilde{G}_N(x)$ is obtained directly from $\tilde{L}_N(x)$. The proof is thus completed. \square

By Theorem 5.2 we see that Algorithm 2.1 is of second-order convergence and that N must increase with the wave number k increasing if the same level of accuracy is required. Thus, the computational complexity will be increased as k increases in order to get the same level accuracy.

Remark 5.3. *Algorithm 2.1 is only of second-order accuracy due to the accuracy of FFT. FFT with higher-order accuracy can be achieved by multiplying the integrand with a weight function. Then, by removing more terms in (2.3), we can obtain an algorithm of higher-order convergence. Note that the second-order accuracy is usually enough for integral equation methods.*

5.2 The three-dimensional case

We now consider the convergence of Algorithm 3.1 in the three-dimensional case. First, we will consider the convergence of the series (3.7). The following result is achieved by using the representation of \hat{L}_{dj} .

Theorem 5.4. *For any $m \in \mathbb{N}^+$, suppose $\mathcal{X}, \mathcal{Y}_\varepsilon \in C^{m+3}$. For any wavenumber $k > 0$ and positive integer N , L_N converges uniformly to L with m -th order accuracy as $N \rightarrow 0$, that is,*

$$\|L_{dN} - L_d\|_{L^\infty(D_c)} \leq CN^{-m} \quad (5.1)$$

where C is a constant depending on $\|\mathcal{X}^{(m+3)}\|_{L_1[-\tilde{c}, \tilde{c}]}$, $\|\mathcal{Y}_\varepsilon^{(n)}\|_{L_1[-\tilde{c}, \tilde{c}]}$, $1 \leq n \leq m+3$, and k .

Proof. From $\hat{L}_{dj} = \hat{K}_{dj} - \hat{F}_j$, \hat{L}_{dj} has three terms. Set

$$\begin{aligned} \hat{L}_{dj} &= \frac{1}{\sqrt{8\pi^2\tilde{c}}} \left[\frac{1}{2\beta_{j_1,j_2}(j_3\pi/\tilde{c} - \beta_{j_1,j_2})} L_{1,j} - \frac{1}{2\beta_{j_1,j_2}(j_3\pi/\tilde{c} + \beta_{j_1,j_2})} L_{2,j} \right. \\ &\quad \left. + \frac{1}{(\alpha_1 + j_1)^2 + (\alpha_2 + j_2)^2 + (j_3\pi/\tilde{c})^2 - k^2} L_{3,j} \right] \end{aligned}$$

where

$$\begin{aligned} L_{1,j} &= \int_{-\tilde{c}}^{\tilde{c}} \exp[i(\beta_{j_1,j_2} - j_3\pi/\tilde{c})x_3] \mathcal{X}'(x_3) dx_3 \\ L_{2,j} &= \int_{-\tilde{c}}^{\tilde{c}} \exp[-i(\beta_{j_1,j_2} + j_3\pi/\tilde{c})x_3] \mathcal{X}'(-x_3) dx_3 \\ L_{3,j} &= \int_{D_{\tilde{c}}} \frac{e^{ik|x|}}{4\pi|x|} (2ik\mathcal{Y}_\varepsilon'(|x|) + \mathcal{Y}_\varepsilon''(|x|)) \exp[-i(\alpha_1 j_1 x_2 + \alpha_2 j_2 x_2 + j_3\pi x_3/\tilde{c})] dx \end{aligned}$$

First consider $L_{1,j}$. By integration by parts, we have:

$$L_{1,j} = \frac{i^{m+2}}{(\beta_{j_1,j_2} - j_3\pi/\tilde{c})^{m+2}} \int_{-\tilde{c}}^{\tilde{c}} \exp[i(\beta_{j_1,j_2} - j_3\pi/\tilde{c})x_3] \mathcal{X}^{(m+3)}(x_3) dx_3$$

then

$$|L_{1,j}| \leq \begin{cases} \frac{1}{|\beta_{j_1,j_2} - j_3\pi/\tilde{c}|^{m+2}} \|\mathcal{X}^{(m+3)}\|_{L_1[-\tilde{c},\tilde{c}]}, & \text{if } \text{Im}(\beta_{j_1,j_2})=0, \\ \frac{e^{-|\beta_{j_1,j_2}|c}}{|\beta_{j_1,j_2} - j_3\pi/\tilde{c}|^{m+2}} \|\mathcal{X}^{(m+3)}\|_{L_1[-\tilde{c},\tilde{c}]}, & \text{if } \text{Re}(\beta_{j_1,j_2})=0. \end{cases}$$

The estimation of $L_{2,j}$ can be obtained similarly.

$$|L_{2,j}| \leq \begin{cases} \frac{1}{|\beta_{j_1,j_2} + j_3\pi/\tilde{c}|^{m+2}} \|\mathcal{X}^{(m+3)}\|_{L_1[-\tilde{c},\tilde{c}]}, & \text{if } \text{Im}(\beta_{j_1,j_2})=0, \\ \frac{e^{-|\beta_{j_1,j_2}|c}}{|\beta_{j_1,j_2} + j_3\pi/\tilde{c}|^{m+2}} \|\mathcal{X}^{(m+3)}\|_{L_1[-\tilde{c},\tilde{c}]}, & \text{if } \text{Re}(\beta_{j_1,j_2})=0. \end{cases}$$

Now consider $L_{3,j}$. Define $h(x) = \frac{e^{ik|x|}}{4\pi|x|} (2ik\mathcal{Y}'_\varepsilon(|x|) + \mathcal{Y}''_\varepsilon(|x|)) e^{-i\alpha_1 x_1 - i\alpha_2 x_2}$, then

$$|L_{3,j}| \leq \frac{1}{|j|^{m+1}} \|h^{(m+1)}\|_{L_1(D_{\tilde{c}})}$$

Note that $h^{(m+1)}$ is composed by $\mathcal{Y}^{(n)}$, $1 \leq n \leq m+3$. Define the set

$$T_N = \{n \in \mathbb{Z} : -N \leq n < N\}$$

For a sufficient large integer N , when $j_1, j_2 \notin T_{N-1}$, β_{j_1,j_2} is a pure imaginary number. Define

$$\begin{aligned} D_{1,N} &= \{(n_1, n_2, n_3) \in \mathbb{Z}^3 : n_1, n_2 \in T_N, n_3 \notin T_N\} \\ D_{2,N} &= \{(n_1, n_2, n_3) \in \mathbb{Z}^3 : n_1, n_2 \notin T_N, n_3 \in \mathbb{Z}\} \end{aligned}$$

then $\mathbb{Z}^3 \setminus S_N = D_{1,N} \cup D_{2,N}$. If $j \in D_{2,N}$, β_{j_1,j_2} is a pure imaginary number. Suppose $|\beta_{j_1,j_2}|$ has a lower boundary such that $|\beta_{j_1,j_2}| \geq b > 0$, $\forall j_1, j_2 \in \mathbb{Z}$.

With the results above, we can estimate the distance between L_N and L.

$$\begin{aligned} |L_d(x) - L_{dN}(x)| &= \left| \sum_{j \in \mathbb{Z}^3 \setminus S_N} \hat{L}_{dj} \phi_j(x) \right| = \left| \sum_{j \in D_{1,N}} \hat{L}_{dj} \phi_j(x) + \sum_{j \in D_{2,N}} \hat{L}_{dj} \phi_j(x) \right| \\ &\leq \frac{1}{8\pi^2 \tilde{c}} \sum_{j \in D_{1,N}} |\hat{L}_{dj}| + \frac{1}{8\pi^2 \tilde{c}} \sum_{j \in D_{2,N}} |\hat{L}_{dj}| \\ &\leq \frac{1}{8\pi^2 \tilde{c}} \sum_{j \in D_{1,N}} \left[\frac{|L_{1,j}|}{2b|j_3\pi/\tilde{c} - \beta_{j_1,j_2}|} + \frac{|L_{2,j}|}{2b|j_3\pi/\tilde{c} + \beta_{j_1,j_2}|} \right] \\ &\quad + \frac{1}{8\pi^2 \tilde{c}} \sum_{j \in D_{2,N}} \left[\frac{|L_{1,j}|}{2b|j_3\pi/\tilde{c} - \beta_{j_1,j_2}|} + \frac{|L_{2,j}|}{2b|j_3\pi/\tilde{c} + \beta_{j_1,j_2}|} \right] \\ &\quad + \frac{1}{8\pi^2 \tilde{c}} \sum_{j \notin S_N} \frac{|L_{3,j}|}{|(\alpha_1 + j_1)^2 + (\alpha_2 + j_2)^2 + (j_3\pi/\tilde{c})^2 - k^2|} \end{aligned}$$

Consider the first term. Note that $\forall j_1, j_2 \in \mathbb{Z}$, $0 \leq \operatorname{Re}(\beta_{j_1, j_2}) \leq k$. When N is sufficient large, $|\beta_{j_1, j_2} - j_3\pi/\tilde{c}| \sim |j_3\pi/\tilde{c}|$, for any $j \in D_{1, N}$. We omit the constants, then

$$\begin{aligned} \sum_{j \in D_{1, N}} \frac{|L_{1, j}|}{|j_3\pi/\tilde{c} - \beta_{j_1, j_2}|} &\leq \sum_{j \in D_{1, N}} \frac{\|\mathcal{X}^{(m+3)}\|_{L_1[-\tilde{c}, \tilde{c}]} }{|\beta_{j_1, j_2} - j_3\pi/\tilde{c}|^{m+3}} \sim \sum_{j_1, j_2 \in T_N} \sum_{j_3 \notin T_N} \frac{\|\mathcal{X}^{(m+3)}\|_{L_1[-\tilde{c}, \tilde{c}]} }{|j_3\pi/\tilde{c}|^{m+3}} \\ &\leq 4N^2 \sum_{|j_3| \geq N} \frac{\|\mathcal{X}^{(m+3)}\|_{L_1[-\tilde{c}, \tilde{c}]} }{|j_3\pi/\tilde{c}|^{m+3}} \leq CN^2 \frac{1}{N^{m+2}} = CN^{-m} \end{aligned}$$

The estimation of the second term is similar:

$$\sum_{j \in D_{1, N}} \frac{|L_{2, j}|}{|j_3\pi/\tilde{c} + \beta_{j_1, j_2}|} \leq CN^{-m}$$

Consider the third term. For $j \in D_{2, N}$, β_{j_1, j_2} is a pure imaginary number and $\operatorname{Im}(\beta_{j_1, j_2}) = O(|j|)$, so $|j_3\pi/\tilde{c} - \beta_{j_1, j_2}| \sim \sqrt{(j_3\pi/\tilde{c})^2 + |j|^2}$. Then

$$\begin{aligned} \sum_{j \in D_{2, N}} \frac{|L_{1, j}|}{|j_3\pi/\tilde{c} - \beta_{j_1, j_2}|} &\leq \sum_{j \in D_{2, N}} \frac{e^{-|\beta_{j_1, j_2}|c} \|\mathcal{X}^{(m+3)}\|_{L_1[-\tilde{c}, \tilde{c}]} }{|\beta_{j_1, j_2} - j_3\pi/\tilde{c}|^{m+3}} \sim \sum_{j_1, j_2 \notin T_N} \sum_{j_3 \in \mathbb{Z}} \frac{e^{-|j|c} \|\mathcal{X}^{(m+3)}\|_{L_1[-\tilde{c}, \tilde{c}]} }{[(j_3\pi/\tilde{c})^2 + |j|^2]^{\frac{m+3}{2}}} \\ &\leq C \sum_{|j_1|, |j_2| \geq N} \frac{e^{-|j|c} \|\mathcal{X}^{(m+3)}\|_{L_1[-\tilde{c}, \tilde{c}]} }{N^{m+2}} \leq Ce^{-cN} \end{aligned}$$

Similar result is obtained for the fourth term:

$$\sum_{j \in D_{2, N}} \frac{|L_{2, j}|}{|j_3\frac{\pi}{\tilde{c}} + \beta_{j_1, j_2}|} \leq Ce^{-cN}$$

The estimate for the last term is trivial, and we will not explain in detail here:

$$\sum_{j \in \mathbb{Z}^3 \setminus S_N} \frac{|L_{3, j}|}{|(\alpha_1 + j_1)^2 + (\alpha_2 + j_2)^2 + (j_3\frac{\pi}{\tilde{c}})^2 - k^2|} \sim \sum_{j \in \mathbb{Z}^3 \setminus S_N} \frac{\|h^{(m+1)}\|_{L_1(D_{\tilde{c}})}}{|j|^{m+3}} \leq CN^{-m}$$

Then we can get the final estimate of $|L_N(x) - L(x)|$:

$$|L_d(x) - L_{dN}(x)| \leq (CN^{-m} + CN^{-m} + Ce^{-cN} + Ce^{-cN} + CN^{-m}) \leq CN^{-m}$$

The proof is completed. \square

Theorem 5.5. For any $x \in D_{dc}$, the error between the exact value $G_d(x)$ and the numerical value $\tilde{G}_{dN}(x)$ obtained by Algorithm 3.1 satisfies the following estimate:

$$|G_d(x) - \tilde{G}_{dN}(x)| = O\left(\frac{1}{N^\sigma}\right) \quad (5.2)$$

where $\sigma = \min\{2, m\}$.

Proof. By Theorem 5.4, we have that at any grid point x^*

$$|L_d(x^*) - L_{dN}(x^*)| \leq CN^{-m}$$

Note that the procedure of computing $L_{dN}(x^*)$ makes use of FFT to compute the Fourier coefficients of L_d with the error bounded by CN^{-2} . So the value we actually obtain is $\tilde{L}_{dN}(x^*)$ with Fourier coefficients \hat{L}_{dj} satisfying that $|\hat{L}_{dj} - \tilde{L}_{dj}|/|\hat{L}_{dj}| \leq CN^{-2}$. Thus we have

$$|L_d(x^*) - \tilde{L}_{dN}(x^*)| \leq |L_d(x^*) - L_{dN}(x^*)| + |L_{dN}(x^*) - \tilde{L}_{dN}(x^*)| \leq CN^{-m} + CN^{-2} = CN^{-\sigma}$$

For any $x \in D_{dc}$, the value $\tilde{L}_{dN}(x)$ is obtained by tri-cubic interpolation with the interpolation error CN^{-4} . Then

$$|L_d(x) - \tilde{L}_{dN}(x)| \leq CN^{-\sigma}(1 + CN^{-4}) = CN^{-\sigma}$$

The required error estimate then follows from this since $\tilde{G}_{dN}(x)$ is obtained directly from $\tilde{L}_{dN}(x)$. The proof is completed. \square

Remark 5.6. *From Theorem 5.5, Algorithm 3.1 is of σ -th order accuracy, and σ is the smaller one between m and 2. This shows that if $m \geq 2$, the algorithm is of second order. So if we need higher accuracy, we should choose sufficient smooth functions $\mathcal{X}, \mathcal{Y}_\varepsilon$, and use higher-order accuracy FFT method.*

5.3 The Maxwell's equation case

In this section, we will give the convergence and error estimates of Algorithm 4.1 to calculate $\mathbb{G}(x)$. The convergence result of L^{pq} , $p, q = 1, 2, 3$ is a result from Theorem 5.4:

Theorem 5.7. *For any integer $m > 2$, suppose $\mathcal{X}, \mathcal{Y}_\varepsilon \in C^{m+3}$. For any wavenumber $k > 0$ and positive integer N , L_N^{pq} converges uniformly to L^{pq} with $m-2$ -th order accuracy as $N \rightarrow \infty$, that is,*

$$\|L_{dN}^{pq} - L_d^{pq}\|_{L^\infty(D_c)} \leq CN^{-m+2} \quad (5.3)$$

Proof. The proof is similar as the proof of Theorem 5.4, by replacing \hat{L}_{dj} by \hat{L}_{dj}^{pq} . So we omit it here. \square

The error estimate is also easily obtained from Theorem 5.5, and we omit the proof here:

Theorem 5.8. *For any $x \in D_{dc}$, the error between the exact value $\mathbb{G}(x)$ and the numerical value $\tilde{\mathbb{G}}_N(x)$ obtained by Algorithm 4.1 satisfies the following estimate:*

$$\max_{j,l=1,2,3} |\mathbb{G}_{jl}(x) - \tilde{\mathbb{G}}_{jl}(x)| = O\left(\frac{1}{N^\sigma}\right) \quad (5.4)$$

where $\sigma = \min\{2, m-2\}$, A_{jl} stands for the entry of matrix A in the j -th row and l -th column.

6 Numerical examples

In this section, we will present several numerical examples of Algorithm 2.1, 3.1 and 4.1. The FFT-based new method will also be compared to some other efficient numerical methods, to show that this method is competitive when large number of values are needed. In the numerical methods in this section, the cut off functions \mathcal{X} and \mathcal{Y}_ε are both C^8 functions.

6.1 Numerical examples for $G(x)$

In this section, we consider the computation of $G(x)$ in 2D space. We will show the numerical results from Algorithm 2.1 in Section 6.1.1, and the comparison of the FFT-based method with the Lattice sums, the Ewald's method and the NA method in Section 6.1.2. In this section we fix $c = 0.6$, $\tilde{c} = 1$. As is shown in Remark 2.1, the Fourier coefficients $\hat{F}_{1,j}$ and $\hat{F}_{2,j}$ are assumed to be known, they are calculated and saved before any numerical procedures. The calculation was carried out by 2D FFT with 2048×2048 uniform nodal grids in $D_{\tilde{c}}$. All computations are carried out by MATLAB R2012a, on a 2 GHz AMD 3800+ machine with 1 GB RAM.

6.1.1 Examples of the FFT-based method

We will give four examples in this subsection. For each example, we fix k and α , and the Green's function is evaluated at four points $P_1^2 = (0.01\pi, 0)$, $P_2^2 = (0.01\pi, 0.01)$, $P_3^2 = (0.5\pi, 0)$ and $P_4^2 = (0.5\pi, 0.01)$. The relative errors at each points for different N 's are shown in Table 1-4.

Table 1: $k = \sqrt{10}$, $\alpha = 0.3$

	P_1^2	P_2^2	P_3^2	P_4^2
$N = 32$	4.30E - 04	4.60E - 04	5.97E - 05	5.86E - 05
$N = 64$	9.12E - 05	1.12E - 04	4.10E - 06	4.06E - 06
$N = 128$	4.11E - 05	3.74E - 05	3.48E - 07	3.54E - 07
$N = 256$	2.87E - 07	6.82E - 07	4.60E - 07	4.62E - 07
$N = 512$	4.08E - 07	3.48E - 07	4.57E - 07	4.58E - 07
$N = 1024$	1.70E - 07	1.66E - 07	4.57E - 07	4.58E - 07

Table 2: $k = 5$, $\alpha = 0.3$

	P_1^2	P_2^2	P_3^2	P_4^2
$N = 32$	1.63E - 03	1.72E - 03	7.63E - 05	7.63E - 05
$N = 64$	2.67E - 04	3.31E - 04	1.52E - 06	1.46E - 06
$N = 128$	1.22E - 04	1.11E - 04	5.98E - 07	6.19E - 07
$N = 256$	6.16E - 07	1.82E - 06	6.90E - 07	6.97E - 07
$N = 512$	9.61E - 07	7.93E - 07	6.95E - 07	6.95E - 07
$N = 1024$	2.59E - 07	2.55E - 07	6.95E - 07	6.95E - 07

Table 3: $k = 50$, $\alpha = \sqrt{2}$

	P_1^2	P_2^2	P_3^2	P_4^2
$N = 128$	3.96E - 02	3.66E - 02	2.28E - 04	1.84E - 04
$N = 256$	1.81E - 03	2.07E - 03	1.53E - 05	9.71E - 06
$N = 512$	2.45E - 04	2.30E - 04	6.84E - 06	6.64E - 06
$N = 1024$	3.20E - 05	3.41E - 05	6.62E - 06	6.62E - 06

Table 4: $k = 100, \alpha = -\sqrt{2}$

	P_1^2	P_2^2	P_3^2	P_4^2
$N = 256$	3.89E - 02	3.75E - 02	1.44E - 04	6.40E - 05
$N = 512$	2.76E - 03	2.82E - 03	4.75E - 06	8.76E - 06
$N = 1024$	4.72E - 04	4.26E - 04	8.95E - 06	9.37E - 06

From examples above, it is shown that Algorithm 2.1 is convergent. When N is relatively small, the relative errors decay at the rate shown in Section 5.1. When N gets larger, the relative errors do not decay as expected, as the 2D FFT algorithm to compute the Fourier coefficients $\hat{F}_{1,j}$ and $\hat{F}_{2,j}$ has a error level of $\frac{1}{2048^2} \sim 10^{-7}$.

The preparation time increases as N increases, and is the most time-consuming part in the numerical procedure. The time cost by the preparation step for $N = 32, 64, 128, 256$ are around 3.5 seconds, for $N = 512$ is 4.5 seconds and for $N = 1024$ is 7.5 seconds, on average. So the preparation time increase as N increases, but it increase slowly and does not take up too much time. Moreover, the preparation step only needs to run once at the beginning of the whole numerical scheme.

On the other hand, the calculation time does not depend on N . In the examples above, it takes about 8.5×10^{-5} seconds on average. Thus the calculation step a very efficient scheme, and quite suitable for large amount of evaluations.

6.1.2 Comparison with other methods

In this subsection, we will compare the FFT-based method (FM in tables) with the Lattice sums (LS in tables), the Ewald's method (EM in tables), and the NA₁ method from [10].

First, four groups of examples are given to compare the FFT-based method with the Lattice sums and the Ewald's method. In each group, we calculate the Green's function with fixed k and α , at the four points P_1^2, P_2^2, P_3^2 and P_4^2 . Similar to the FFT-based method, the Lattice sums also have two steps, i.e., the preparation step and the calculation step. As the preparation step takes up no more than 1 minute, we omit the preparation times. We adjust the parameters in each method to achieve similar accuracies. If any of the methods fails to achieve the required accuracy, we will choose the parameters such that the method could achieve the best accuracy. We will show the relative errors and calculation times in Table 5-8.

Table 5: $k = 5, \alpha = 0.3$

	P_1^2		P_2^2		P_3^2		P_4^2	
	r-error	c-time(s)	r-error	c-time(s)	r-error	c-time(s)	r-error	c-time(s)
LS	3E - 07	8.6E - 4	6E - 07	8.6E - 4	4E - 07	3.1E - 3	4E - 06	1.4E - 3
EM	4E - 07	1.9E - 3	4E - 07	2.0E - 3	3E - 07	1.9E - 3	3E - 07	1.9E - 3
FM	9E - 07	9.9E - 5	8E - 07	9.2E - 5	7E - 07	9.2E - 5	7E - 07	8.8E - 5

Table 6: $k = 50, \alpha = \sqrt{2}$

	P_1^2		P_2^2		P_3^2		P_4^2	
	r-error	c-time(s)	r-error	c-time(s)	r-error	c-time(s)	r-error	c-time(s)
LS	5E-05	9.0E-4	2E-05	1.1E-3	2E-01	1.4E-3	2E-01	1.4E-3
EM	2E-05	3.0E-3	2E-05	3.7E-3	8E-06	3.0E-3	8E-06	3.0E-3
FM	3E-05	8.6E-5	3E-05	9.0E-5	7E-06	8.7E-5	7E-06	9.0E-5

Table 7: $k = 100, \alpha = 0.5$

	P_1^2		P_2^2		P_3^2		P_4^2	
	r-error	c-time(s)	r-error	c-time(s)	r-error	c-time(s)	r-error	c-time(s)
LS	1E-04	1.2E-3	1E-04	1.2E-3	9E-01	1.3E-3	9E-01	1.2E-3
EM	2E-04	3.4E-3	2E-04	3.4E-3	9E-06	4.7E-3	9E-06	3.6E-3
FM	4E-04	9.2E-5	4E-04	8.8E-5	1E-05	8.5E-5	1E-05	9.2E-5

Table 8: $k = 200, \alpha = 0.8$

	P_1^2		P_2^2		P_3^2		P_4^2	
	r-error	c-time(s)	r-error	c-time(s)	r-error	c-time(s)	r-error	c-time(s)
LS	1E-02	1.4E-3	1E-02	1.3E-3	6E-01	1.2E-3	6E-01	1.0E-3
EM	2E-03	4.4E-3	2E-03	4.6E-3	1E-05	4.5E-3	1E-05	5.3E-3
FM	4E-03	8.9E-5	4E-03	8.5E-5	7E-06	8.3E-5	8E-06	8.3E-5

From the four examples, when k gets larger, the Lattice sums needs more time to reach the required accuracy, or even fails to work when the point is not too close to 0. When k and r are both small enough, it is faster than the Ewald's method, and much slower than the FFT-based method. On the other hand, the Ewald's method can reach any accuracy if required, but its speed is not so competitive. The FFT-based method is the fastest during the calculation step, despite that it takes about 4 seconds in the first example ($N = 512$), and about 7.5 seconds in the second to forth examples ($N = 1024$) to do the preparation before that. This leads to the conclusion that when k is small enough, the FFT-based method is more competitive, while when k is larger, the FFT-based method wins if large amount of values are needed, but if the number of evaluations is small or a very high accuracy is required, the Ewald's method is a better choice.

We also compare our method with the so-called NA method shown in [10]. In that paper, the authors introduced three methods, NA₁, NA₂ and NA₃, to calculate the quasi-periodic Green's functions for very high wave numbers, i.e. $k \geq 10^4$. We only compare the FFT-based method with NA₁ here, for the three methods performs similarly when k is not very high. Examples are taken when $k = 10.2, 100.2, 200.2$, at the points $(0, 0.01)$ and $(0, 0.1)$. Similar to the examples before, we choose proper parameters such that both of the two methods can achieve similar relative errors.

Table 9: Comparision with NA_1

k	point	NA_1		FM	
		r-error	c-time(s)	r-error	c-time(s)
10.2	(0, 0.01)	1E-08	0.045	7E-09	0.000087
10.2	(0, 0.1)	1E-07	0.045	3E-07	0.000089
100.2	(0, 0.01)	1E-05	0.046	1E-05	0.000087
100.2	(0, 0.1)	7E-06	0.043	4E-06	0.000084
200.2	(0, 0.01)	6E-05	0.046	8E-05	0.000083
200.2	(0, 0.1)	1E-05	0.040	6E-05	0.000086

From Table 9, the FFT-based method is much faster than NA_1 . But note that NA_1 also has its advantage, that it can reach a much higher rate of accuracy without costing more time. It also works well for very large k 's, when the FFT-based method takes up too much time and memory to achieve the same accuracy. When the wave number k is not that large, i.e., $k \sim 100$, the FFT-based method is more competitive if large number of values are needed.

6.2 Numerical examples for $G_d(x)$

In this subsection, we will show some numerical examples of the calculation of $G_d(x)$ in 3D space by Algorithm 3.1. We will give the examples to show the results from our methods in Subsection 6.2.1, and the comparison of our method with the Lattice sum and the Ewald method in Subsection 6.2.2. In this section we fix $c = 0.6$, $\tilde{c} = 1$. Our numerical procedure in this section is ran by Fortran 11.1.064, on a 2.40GHz NF560D2 machine with 96 GB RAM.

6.2.1 Examples of the FFT-based method

In this subsection, we will give examples of the FFT-based method to compute the 3D quasi-periodic Green's function $G_d(x)$. We will show six groups of examples. In each group, the wave number k is fixed, and the values at four points $P_1^3 = (0, 1.5, 0.0008)$, $P_2^3 = (0.03, 0.03, 0.0008)$, $P_3^3 = (0, 1.5, 0.1)$ and $P_4^3 = (0.03, 0.03, 0.1)$ are evaluated for different N 's. The eigenfunction expansion (1.3) with sufficiently large number of terms is used to compute the "exact value" of $G_d(x)$. The the relative errors of values calculated at each point with different N 's are shown in Table 10-15.

Table 10: $k = 1$, $\alpha_1 = 0.1$, $\alpha_2 = 0.2$

	P_1^3	P_2^3	P_3^3	P_4^3
$N = 32$	3.73E - 04	6.97E - 05	3.94E - 04	1.72E - 04
$N = 64$	1.18E - 07	1.24E - 07	1.20E - 07	1.88E - 07
$N = 128$	3.59E - 07	7.29E - 09	3.54E - 07	1.88E - 08
$N = 256$	5.48E - 08	2.52E - 10	5.39E - 08	6.53E - 10
$N = 512$	1.38E - 09	9.67E - 12	1.32E - 09	2.49E - 10

Table 11: $k = 5, \alpha_1 = 0.1, \alpha_2 = 0.2$

	P_1^3	P_2^3	P_3^3	P_4^3
$N = 32$	7.76E - 04	1.20E - 04	6.81E - 04	2.89E - 04
$N = 64$	6.44E - 05	4.58E - 06	6.43E - 05	1.17E - 05
$N = 128$	1.01E - 05	9.31E - 07	9.83E - 06	2.42E - 06
$N = 256$	1.55E - 06	3.23E - 08	1.51E - 06	8.39E - 08
$N = 512$	4.58E - 08	1.17E - 08	4.50E - 08	3.05E - 08

Table 12: $k = 10, \alpha_1 = 0.8, \alpha_2 = \sqrt{2}$

	P_1^3	P_2^3	P_3^3	P_4^3
$N = 32$	3.49E - 02	1.22E - 03	3.33E - 02	3.16E - 03
$N = 64$	1.99E - 03	5.17E - 05	1.99E - 03	1.36E - 04
$N = 128$	4.15E - 04	3.76E - 06	4.22E - 04	9.86E - 06
$N = 256$	6.29E - 05	1.81E - 07	6.40E - 05	4.74E - 07
$N = 512$	1.45E - 06	5.16E - 08	1.48E - 06	1.35E - 07

Table 13: $k = 25, \alpha_1 = 0.8, \alpha_2 = \sqrt{2}$

	P_1^3	P_2^3	P_3^3	P_4^3
$N = 64$	3.97E - 02	1.48E - 03	3.94E - 02	3.63E - 03
$N = 128$	3.35E - 03	6.04E - 05	3.78E - 03	1.49E - 04
$N = 256$	4.99E - 04	6.19E - 06	5.65E - 04	1.53E - 05
$N = 512$	7.86E - 06	6.53E - 07	9.55E - 06	1.60E - 06

Table 14: $k = 50, \alpha_1 = \sqrt{3}, \alpha_2 = 0.5$

	P_1^3	P_2^3	P_3^3	P_4^3
$N = 128$	3.09E - 02	2.26E - 04	2.74E - 02	5.48E - 04
$N = 256$	5.05E - 03	2.29E - 05	4.51E - 03	5.76E - 05
$N = 512$	2.52E - 04	1.46E - 06	2.34E - 04	3.04E - 06
$N = 736$	1.03E - 04	1.72E - 07	9.26E - 05	3.67E - 07

Table 15: $k = 100, \alpha_1 = \sqrt{3}, \alpha_2 = 0.5$

	P_1^3	P_2^3	P_3^3	P_4^3
$N = 128$	7.80E - 02	5.48E - 03	1.05E - 01	1.55E - 02
$N = 256$	9.68E - 03	1.13E - 03	1.56E - 02	3.14E - 03
$N = 512$	1.15E - 03	4.01E - 05	5.74E - 04	1.02E - 04
$N = 736$	1.31E - 04	3.64E - 06	1.94E - 04	9.27E - 06

From these examples above, Algorithm 3.1 is convergent with the relative errors bounded by that estimated in Section 5.2. Although the convergence of the algorithm is quite fast, as is

shown in Section 5.2, when k is large, N should be larger to achieve a acceptable accuracy.

Similar to the 2D case, the preparation step is the most time-consuming part in the numerical scheme, and the time taken up by this step depends on N . The following figure gives the relationship between the average preparation time and N .

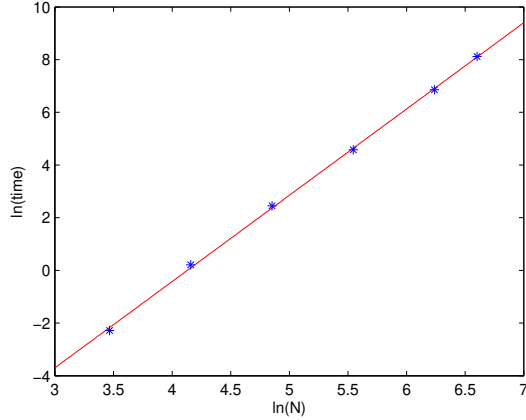


Figure 1: preparation time

The blue stars are the data and the red line is the linear fitting of the data. From the Figure 1, the preparation time increases at the rate of $N^{3.3}$, as N increases. It increase significantly when N gets larger.

Fortunately, the preparation step needs to be ran only once, before the calculation step starts. The calculation step takes up about 1.3×10^{-6} seconds on average, which does not depend on any parameter. This is a quite efficient step, which is very suitable for large amount of evaluations.

6.2.2 Comparison with other methods

In this subsection, we will compare the FFT-based method (FM) with the Ewald method (EM) and the Lattice sums (LS). We will apply these three methods to six examples with different k 's at the points P_1^3 and P_2^3 . Not the same as the 2D case, the preparation times are no long too small to be ignored. In Table 16-21, we list the relative errors and the preparation time (p-time) and calculation times (c-time) in the case that $k = 1, 5, 10, 25, 50, 100$. The parameter N in the FFT-based method is changed when k is different.

Table 16: $k = 1, N = 32$

	P_1^3		P_2^3		p-time(s)
	r-error	c-time(s)	r-error	c-time(s)	
EM	3.60E - 05	1.00E - 3	1.02E - 06	1.00E - 3	0
LS	4.29E - 02	6.90E - 5	2.39E - 05	6.90E - 5	13.4
FM	3.73E - 04	1.30E - 6	6.97E - 05	1.29E - 6	0.10

Table 17: $k = 5, N = 64$

	P_1^3		P_2^3		p-time(s)
	r-error	c-time(s)	r-error	c-time(s)	
EM	4.09E - 05	1.40E - 2	3.38E - 06	1.40E - 2	0
LS	2.81E - 03	6.90E - 5	2.99E - 06	6.80E - 5	14
FM	6.44E - 05	1.28E - 6	4.58E - 06	1.29E - 6	1.24

Table 18: $k = 10, N = 128$

	P_1^3		P_2^3		p-time(s)
	r-error	c-time(s)	r-error	c-time(s)	
EM	8.01E - 04	5.20E - 2	3.19E - 05	4.90E - 2	0
LS	1.00E - 04	1.80E - 4	1.91E - 05	1.82E - 4	34
FM	4.15E - 04	1.30E - 6	3.76E - 06	1.30E - 6	11.42

Table 19: $k = 25, N = 256$

	P_1^3		P_2^3		p-time(s)
	r-error	c-time(s)	r-error	c-time(s)	
EM	2.26E - 04	0.33	1.31E - 05	0.32	0
LS	2.89E - 04	6.65E - 4	2.34E - 04	6.68E - 4	125
FM	4.99E - 04	1.28E - 6	6.19E - 06	1.30E - 6	96.2

Table 20: $k = 50, N = 512$

	P_1^3		P_2^3		p-time(s)
	r-error	c-time(s)	r-error	c-time(s)	
EM	1.75E - 04	1.22	5.96E - 05	1.21	0
LS	4.15E - 02	2.33E - 3	6.68E - 04	2.34E - 3	811
FM	2.52E - 04	1.31E - 6	1.46E - 06	1.28E - 6	940

Table 21: $k = 100, N = 736$

	P_1^3		P_2^3		p-time(s)
	r-error	c-time(s)	r-error	c-time(s)	
EM	2.59E - 04	5.32	2.75E - 06	6.44	0
LS	7.79E - 01	1.62E - 3	6.23E - 03	1.63E - 3	828
FM	1.31E - 04	1.29E - 6	3.64E - 06	1.30E - 6	3322

From the tables above, the Ewald's method is able to achieve any required accuracy and does not have any preparation time. However, the calculation time taken up by this method grows significantly as k increases. Similar to 2D case, the Lattice sums also suffers from the problems of convergence, when k is relatively larger. The calculation time of this method is much less than

the Ewald method, but still more than the FFT-based method. The FFT-based method is the fastest and works well for all k 's with a dependent calculation time. However, when k increases, larger N is required for accuracy, which leads to a significant growth in the preparation time and memory. Thus when a small number of values or high accuracies are needed, the Ewald's method is the best choice, while if large amount of evaluations is required, the FFT-based method is more competitive.

6.3 Numerical examples for $\mathbb{G}(x)$

In this section, we will show some numerical examples for the calculation of $\mathbb{G}(x)$ by Algorithm 4.1. We will present six numerical examples to show the efficiency of this algorithm. The maximum relative errors (i.e. $\max_{j,l=1,2,3} \frac{|\mathbb{G}_{jl}(x) - \tilde{\mathbb{G}}_{jl}(x)|}{|\mathbb{G}_{jl}(x)|}$), are calculated at each point for $N = 32, 64, 128, 256, 512$ are shown Table 22-27.

Table 22: $k = 1, \alpha_1 = 0.1, \alpha_2 = 0.2$

	P_1^3	P_2^3	P_3^3	P_4^3
$N = 32$	1.09E - 02	2.65E - 06	3.42E - 01	4.18E - 04
$N = 64$	9.00E - 06	6.96E - 08	2.49E - 04	8.82E - 06
$N = 128$	2.50E - 06	3.04E - 10	6.99E - 06	1050E - 08
$N = 256$	5.61E - 07	1.12E - 11	3.61E - 07	3.55E - 11
$N = 512$	4.71E - 07	5.14E - 12	9.90E - 09	1.48E - 11

Table 23: $k = 5, \alpha_1 = 0.1, \alpha_2 = 0.2$

	P_1^3	P_2^3	P_3^3	P_4^3
$N = 32$	6.92E - 03	6.25E - 05	4.12E - 02	3.86E - 04
$N = 64$	8.84E - 05	2.39E - 06	8.85E - 05	5.56E - 06
$N = 128$	2.49E - 05	4.93E - 07	2.42E - 05	1.16E - 06
$N = 256$	3.81E - 06	1.71E - 08	3.68E - 06	4.07E - 08
$N = 512$	1.26E - 07	6.19E - 09	9.24E - 08	1.44E - 08

Table 24: $k = 10, \alpha_1 = 0.8, \alpha_2 = \sqrt{2}$

	P_1^3	P_2^3	P_3^3	P_4^3
$N = 32$	1.48E - 01	1.00E - 03	1.36E - 01	2.74E - 03
$N = 64$	2.12E - 03	4.24E - 05	2.24E - 03	1.31E - 04
$N = 128$	4.41E - 04	3.09E - 06	4.56E - 04	1.16E - 05
$N = 256$	6.68E - 05	1.48E - 07	6.91E - 05	4.63E - 07
$N = 512$	1.53E - 06	4.23E - 08	1.60E - 06	1.59E - 07

Table 25: $k = 25$, $\alpha_1 = 0.8$, $\alpha_2 = \sqrt{2}$

	P_1^3	P_2^3	P_3^3	P_4^3
$N = 64$	4.53E – 02	1.51E – 03	4.47E – 02	6.22E – 03
$N = 128$	4.62E – 03	6.64E – 05	5.12E – 03	2.54E – 04
$N = 256$	6.93E – 04	6.34E – 06	7.70E – 04	2.62E – 05
$N = 512$	1.32E – 05	6.67E – 07	1.52E – 05	2.74E – 06

Table 26: $k = 50$, $\alpha_1 = \sqrt{3}$, $\alpha_2 = 0.5$

	P_1^3	P_2^3	P_3^3	P_4^3
$N = 128$	3.20E – 02	7.35E – 04	2.78E – 02	1.69E – 03
$N = 256$	5.28E – 03	5.93E – 05	4.55E – 03	1.65E – 04
$N = 512$	2.69E – 04	6.80E – 06	2.43E – 04	1.21E – 05
$N = 736$	1.09E – 04	8.00E – 07	9.37E – 05	1.43E – 06

Table 27: $k = 100$, $\alpha_1 = \sqrt{3}$, $\alpha_2 = 0.5$

	P_1^3	P_2^3	P_3^3	P_4^3
$N = 256$	2.00E – 02	1.90E – 03	4.68E – 02	1.46E – 02
$N = 512$	2.22E – 03	4.13E – 05	1.54E – 03	4.73E – 04
$N = 736$	2.35E – 04	4.69E – 06	5.88E – 04	4.30E – 05

From the examples above, similar results can be concluded as that in Subsection 6.2.1. We does not show the preparation and calculation time as they are both about six times longer than those in Algorithm 3.1. This implies that our method for the calculation of $\mathbb{G}(x)$ is still of high efficiency, especially when large number of values are needed.

Acknowledgements

This work was partly supported by the NNSF of China grants 91430102 and 91630309.

References

- [1] T. Arens, K. Sandfort, S. Schmitt and A. Lechleiter 2013 Analysing Ewald’s method for the evaluation of Green’s functions for periodic media, *IMA J. Numer. Anal.*, **78(3)** 405-431.
- [2] G. Beylkin, C. Kurcz and L. Monzón 2008 Fast algorithms for Helmholtz Green’s functions, *Proc. R. Soc. A.*, **464** 3301-3326.
- [3] O. P. Bruno and B. Delourme 2014 Rapidly convergent two-dimensional quasi-periodic Green function throughout the spectrum ĀĀ including Wood anomalies, *J. Comput. Phys.*, **262** 262-290.

[4] O. P. Bruno and A. G. Fernandez-Lado 2017 Rapidly convergent quasi-periodic Green functions for scattering by arrays of cylinders - including Wood anomalies, *Proc. R. Soc. A.*, **473**.

[5] F. Capolino, D.R. Wilton, and W.A. JohnsonZ 2002 Efficient computation of the 2-D Green's function for 1-D periodic structures using the Ewald method, *IEEE Trans. Antennas Propagat.* **53** (4) 2977-2984.

[6] T.F. Eibert, J.L. Volakis, D.R. Wilton, and D.R. Jackson 1999 Hybrid FE/BI modeling of 3-D doubly periodic structures utilizing triangular prismatic elements and an MPIE formulation accelerated by the Ewald transformation, *IEEE Trans. Antennas Propagat.* **47** 843-850.

[7] N. Guerin, S. Enoch, and G. Tayeb 2001 Combined method for the computation of the doubly periodic Green's function, *J. Electrom. Waves Appl.*, **15** 205 - 221.

[8] T. Hohage 2006 Fast numerical solution of the electromagnetic medium scattering problem and applications to the inverse problem, *J. Comput. Phys.*, **214** 224-238.

[9] R.E. Jorgenson and R. Mittra 1990 Efficient calculation of the free-space periodic Green's function, *IEEE Trans. Antennas Propagat.*, **38** 633 - 642.

[10] H. Kurkcu and F. Reitich 2009 Stable and efficient evaluation of periodized Green's functions for the Helmholtz equation at high frequencies, *J. Comput. Phys.* **228** 75-95.

[11] A. Kustepeli and A.Q. Martin 2000 On the splitting parameter in the Ewald method, *IEEE Microwave Guided Wave Lett.*, **10** 168 - 170.

[12] A. Lechleiter and D. L. Nguyen 2012 Spectral volumetric integral equation methods for acoustic medium scattering in 3D waveguide, *IMA Numer. Anal.*, **32**(3) 813-844.

[13] F. Lekien and J. Marsden 2005 Tricubic interpolation in three dimensions. *Int. J. Numer. Meth. Engng.*, **63** 455-471.

[14] C.M. Linton 1998 The Green's function for the two-dimensional Helmholtz equation in periodic domains, *J. Eng. Math.* **33** 377-402.

[15] C. M. Linton and I. Thompson 2009 One- and two-dimensional lattice sums for the three-dimensional Helmholtz equation, *J. Comput. Phys.*, **228** 1815 - 1829.

[16] C.M. Linton 2010 Lattice Sums for the Helmholtz Equation, *SIAM Rev.* **52** (4) 630-674.

[17] C.M. Linton 2015 Two-dimensional, phase modulated lattice sums with application to the Helmholtz Green's function, *J. Math. Phys.*, **56** 013505.

[18] A.W. Mathis and A.F. Peterson 1998 Efficient electromagnetic analysis of a doubly infinite array of rectangular apertures, *IEEE Trans. Microwave Theory Tech.* **46** 46-54.

[19] A. Moroz 2002 On the computation of the free-space doubly-periodic Green's function of the threedimensional Helmholtz equation, *J. of Electromagn. Waves and Appl.*, **16** 457 - 465.

- [20] A. Moroz 2006 Quasi-periodic Green's functions of the Helmholtz and Laplace equations, *J. Phys.*, **A.39** 11247 - 11282.
- [21] S. Oroskar, D.R. Jackson, and D.R. Wilton 2006 Efficient computation of the 2D periodic Green's function using the Ewald method, *J. Comput. Phys.* **219** 899-911.
- [22] N. A. Ozdemir and C. Craeye 2009 Evaluation of the periodic Green's function near Wood's anomaly and application to the array scanning method, *IEEE Antennas and Propagation Society International Symposium*.
- [23] V. G. Papanicolaou 1999 Ewald's method revisited: Rapidly convergent series representations of certain Green's functions, *J. Comput. Anal. Appl.*, **1** 105 - 114.
- [24] K. Sandfort, *The Factorization Method for Inverse Scattering From Periodic Inhomogeneous Media*, PhD Thesis, KIT, KIT Scientific Publishing, 2010, Germany.
- [25] M. G. Silveirinha and C. A. Fernandes 2005 A new acceleration technique with exponential convergence rate to evaluate periodic Green functions, *IEEE Trans. Antennas Propagat.*, **53** 347 - 355.
- [26] I. Stevanović, P. Crespo-Valero, K. Blagović, F. Bongard, and J.R. Mosig 2006 Integral equation analysis of 3-D metallic objects arranged in 2-D lattices using the Ewald transformation, *IEEE Trans. Microwave Theory Tech.* **54** 3688-3697.
- [27] G. Vainikko, Fast solvers of the Lippmann-Schwinger equation, in: *Direct and Inverse Problems of Mathematical Physics* (eds. R.P. Gilbert, J. Kajiwara and Y. Xu), Kluwer, Dordrecht, The Netherlands, 2000, pp. 423-440.
- [28] G. Valerio, P. Baccarelli, P. Burghignoli, and A. Galli 2007 Comparative analysis of acceleration techniques for 2-D and 3-D Green's functions in periodic structures along one and two directions, *IEEE Trans. Antennas Propagat.* **55** 1630-1643.
- [29] J.A.C. Weideman 1994 Computation of the complex error function, *SIAM.J. Numer Anal* **31(5)** 1497-1518.
- [30] K. Yasumoto and K. Yoshitomi 1999 Efficient calculation of lattice sums for free-space periodic Green's function, *IEEE Trans. Antennas Propagat.*, **47** 1050 - 1055.